Food Chemistry: X 27 (2025) 102424

Contents lists available at ScienceDirect

Food Chemistry: X

journal homepage: www.sciencedirect.com/journal/food-chemistry-x

Unraveling the flavor formation process of mellow and thick-type ripened Pu-erh tea through non-targeted metabolomics and metagenomics

Zixi Yang [a,b,c,1], Yanxia Xie [a,b,c,1], Yuanmin Zhu [a,b,c,*], Mengjie Lei [a,b,c], Xuemin Chen [a,b,c], Wenwen Jin [a,b,c], Chunhua Fu [a,b,c], Longjiang Yu [a,b,c,*]

[a] Institute of Resource Biology and Biotechnology, Department of Biotechnology, College of Life Science and Technology, Huazhong University of Science and Technology, Wuhan 430074, China
[b] Key Laboratory of Molecular Biophysics, Ministry of Education, Wuhan 430074, China
[c] Hubei Engineering Research Center for both Edible and Medicinal Resources, Wuhan 430074, China

ARTICLE INFO

Keywords:
Ripened Pu-erh tea
Flavor formation
Multi-omics analysis
Theabrownins
Functional microbes
Fermentation parameter

ABSTRACT

Ripened Pu-erh tea (RPT) is renowned for its distinctive flavor and health benefits. However, its complex fermentation process poses challenges in ensuring consistency in production. This study investigated RPT flavor formation through sensory evaluation, multi-omics analysis, and multivariate statistical approaches. By day 24, the tea exhibited a reddish-brown infusion and a mellow, thick taste (MT_RPT), achieving the highest sensory score (94.0, $P < 0.05$). Sixteen flavor-related chemical components exhibited significant changes ($P < 0.05$). The contents of free amino acids, *L*-theanine, tea polyphenols, flavonoids, catechins, and thearubigins decreased. In contrast, the contents of total soluble sugars, caffeine, theobromine, epicatechin, and theabrownins (TBs) increased, reaching 74.1 mg/g, 65.38 mg/g, 3.13 mg/g, 3.33 mg/g, and 134.84 mg/g, respectively. Additionally, 33 nonvolatile metabolites (e.g., pelargonidin 3-O-glucoside, dihydroisorhamnetin, and puerarin) were significantly correlated with MT_RPT flavor (VIP > 1, $|r| \geq 0.8$, $P < 0.05$) and influenced by key functional microbes, including *Pantoea*, *Aspergillus*, *Brachybacterium*, and *Staphylococcus*. By day 30, the infusion darkened, and sensory scores declined (81.4, $P < 0.05$), attributed to the dominance of *Brevibacterium*. This microbial shift reduced water-soluble pectin, free amino acids, and 11 metabolites while increasing TBs and theophylline (219.33 mg/g and 0.09 mg/g, respectively). Therefore, TBs were identified as a crucial indicator of optimal fermentation. Moreover, redundancy analysis indicated that the tea pile's central temperature, moisture content, and pH were essential fermentation parameters ($P < 0.05$). These findings deepen our understanding of MT_RPT flavor development mechanisms and provide valuable insights into precise fermentation control.

The list of chemical compounds

PubChem CID	Chemical compounds
370	Gallic acid
2519	Caffeine
5429	Theobromine
65064	Epigallocatechin Gallate
72276	Epicatechin
72277	Epigallocatechin
439378	*L*-Theanine
443648	Pelargonidin 3-O-glucoside
44258022	Isorhamnetin 3-(6''-malonylglucoside)
131751173	Cyanidin 3-glucogalactoside

(*continued on next column*)

(*continued*)

1. Introduction

Ripened Pu-erh tea (RPT), a geographically indicated product from Yunnan, China, is highly valued for its unique flavor and potential health benefits (He et al., 2023; Huang et al., 2019; Wang et al., 2022).

* Corresponding authors at: College of Life Science and Technology, Huazhong University of Science and Technology, No. 1037 Luoyu Road, Wuhan 430074, China.
E-mail address: yulongjiang@hust.edu.cn (L. Yu).
[1] These two authors contributed equally to this work.

https://doi.org/10.1016/j.fochx.2025.102424
Received 19 February 2025; Received in revised form 21 March 2025; Accepted 27 March 2025
Available online 28 March 2025

Made from Yunnan large-leaf sun-dried green tea, the production of RPT involves pile fermentation, drying, and sieving, with pile fermentation playing a crucial role in flavor development (He et al., 2023). Traditional pile fermentation, which comprises spreading and turning sun-dried green tea on a concrete floor, faces industrial challenges such as prolonged processing cycles, high labor demands, and difficulties in process control, leading to inconsistent fermentation quality (Long et al., 2024a). To address these challenges, researchers have developed off-ground fermentation technology, which enhances fermentation efficiency and consistency by precisely controlling temperature, humidity, and ventilation conditions (Ma et al., 2023). Consequently, off-ground fermentation technology has become central to RPT industry research and application.

In the production of RPT, off-ground fermentation primarily involves basket and tank fermentation (Ma et al., 2024a). Basket fermentation involves placing tea leaves in baskets and fermenting them in batches ranging from tens to hundreds of kilograms. Compared to traditional piling fermentation, this method is safer, more hygienic, and requires a shorter fermentation period, but it also reduces the risk of "heap burning" caused by excessive heat accumulation (Li, 2021). Moreover, basket fermentation significantly enhances the transformation of tea chemicals, such as accelerating the degradation of tea polyphenols, theaflavins, catechins, and thearubigins, while increasing caffeine and theabrownins content and reducing "pile odor," which collectively improves tea quality (Wang et al., 2017). Similarly, tank fermentation facilitates the rapid conversion of flavonoids (e.g., kaempferol and quercetin), non-esterified catechins, and gallic acid in RPT (Ma et al., 2023). Tank fermentation using closed containers allows better control over the fermentation process and product stability. However, it necessitates precise regulation of multiple parameters, including temperature, humidity, and oxygen levels (Li et al., 2013). Currently, the mechanisms underlying RPT fermentation and the effects of fermentation parameters remain insufficiently studied. As an intermediary technology between traditional piling and tank fermentation, basket fermentation plays a crucial role in RPT flavor development. Therefore, an in-depth examination of the impact of basket fermentation on RPT flavor and its key influencing factors will not only enhance our understanding of the RPT fermentation mechanism but also provide a theoretical foundation for optimizing parameter control strategies in tank fermentation.

The flavor of RPT is predominantly assessed by its liquid color, aroma, and taste. Among these attributes, liquid color and taste are particularly significant, as they serve as direct indicators of the tea's intrinsic quality (Wang et al., 2022). Intelligent sensory devices, such as colorimeters and electronic tongues, have been employed to simulate human sensory evaluation of tea objectively (Cheng et al., 2021). Furthermore, electron microscopy techniques, including transmission electron microscopy (TEM), scanning electron microscopy (SEM), and others, are widely used for material morphology characterization (Chen et al., 2024; Lin et al., 2024; Wang et al., 2024b), with SEM being ubiquitous in studying tea morphology. While these devices provide valuable objective measurements, they fail to capture the tea flavor's complexity fully. Therefore, a more comprehensive approach is required to elucidate the flavor formation process of RPT more effectively.

In recent years, multi-omics technologies have been widely applied in food, agriculture, and biotechnology (Du et al., 2024; Wang et al., 2024a; Yang et al., 2019). Metabolomics facilitates identifying and quantifying small molecules in biological samples, offering insights into metabolic changes during fermentation (Ma et al., 2024a). Metagenomics, which involves sequencing the genetic material of microbial communities, enables the identification of key functional microbes involved in flavor development (Zhang, Fan, et al., 2024). However, these approaches generate high-dimensional data, resulting in the challenge known as the "curse of dimensionality." To address this, multivariate statistical analyses are extensively utilized (Huang et al., 2022). Principal component analysis (PCA) is commonly used for dimensionality reduction and feature extraction, while two-way orthogonal partial least squares (O2PLS) aid in elucidating inter-dataset relationships (Li et al., 2024; Wang et al., 2018). Therefore, integrating these methods provides a comprehensive approach to elucidating the flavor formation process of RPT.

After conducting multiple batch trials (Fig. S1), our laboratory developed a stable and efficient basket fermentation technique for producing mellow and thick-type RPT (MT_RPT). Building on this foundation, this study employed optimized fermentation parameters and a systematic experimental design to investigate the flavor formation of MT_RPT. A traditional sensory evaluation was first performed to assess flavor changes, while intelligent sensory analysis provided objective, quantitative data on liquid color and taste. The SEM was employed to observe microstructural changes in the tea leaves. High-performance liquid chromatography (HPLC) and non-targeted metabolomics were used to quantify primary chemical constituents and nonvolatile metabolites at different fermentation stages. Metagenomic analysis revealed microbial community dynamics, while multivariate statistical techniques were applied to identify key flavor compounds, core functional microbes, and determinants of microbial succession. This study advances knowledge of MT_RPT flavor formation and provides theoretical guidance for optimizing tank fermentation parameters, contributing to the standardization and stabilization of RPT production.

2. Materials and methods

2.1. Materials and chemicals

The sun-dried green tea, produced from summer-autumn tea leaves (one bud with three leaves), was provided by the Linxiang District Dianhai Ganquan Tea Factory (Lincang, China) for fermentation. The spring water was sourced from Linxiang Xinda Urban Distribution Co., Ltd. (Lincang, China). Standard catechin compounds, including (−)-epigallocatechin gallate (EGCG, ≥98 %), (−)-epigallocatechin (EGC, ≥98 %), (−)-epicatechin gallate (ECG, ≥98 %), (−)-epicatechin (EC, ≥98 %), gallocatechin gallate (GCG, ≥98 %), (−)-gallocatechin (GC, ≥98 %), catechin gallate (CG, ≥98 %), and catechin (C, ≥98 %), as well as caffeine (CAF, ≥98 %), theophylline (≥98 %), theobromine (≥98 %), gallic acid (GA, ≥98 %), and *L*-Theanine (≥98 %), were procured from Shanghai Yuanye Bio-Technology Co., Ltd. (Shanghai, China). Oxalic acid, sodium hydroxide, sodium carbonate, and sodium bicarbonate were sourced from China National Pharmaceutical Group Chemical Reagents Co., Ltd. (Shanghai, China). Additionally, acetonitrile, Folin-Ciocalteu's reagent, ninhydrin, and methanol were sourced from Shanghai McLin Biochemical Technology Co., Ltd. (Shanghai, China), and phenol, Coomassie Brilliant Blue G250, and stannous chloride were sourced from Shanghai Aladdin Biochemical Technology Co., Ltd. (Shanghai, China).

2.2. Preparation of fermented tea samples

The fermentation of MT_RPT was conducted at the Yun Tea Research Engineering Center of the Huaxiang Innovation Research Institute (Lincang, China). Sixty kilograms of raw material were combined with 22 kg of spring water and packed into a wooden basket, which was subsequently covered with damp linen to facilitate fermentation. To ensure uniformity, the tea pile was turned every 6 days. The fermentation process was considered complete when the tea samples displayed a reddish-brown hue (Li, Zhang, et al., 2022). The raw material was designated as sample S0 (day 0), indicating the start of the fermentation process. During the early stage (S1, days 1–6), the center temperature of the tea pile was maintained at 35–45 °C with a moisture content of 35–40 %, and sample S1 was collected on day 6. In the middle stage (S2, days 7–12), the center temperature rose to 50–60 °C, with a moisture content of 37–42 %, and sample S2 was collected on day 12. In the mid-late stage (S3, days 13–18), the center temperature fluctuated between

45 and 55 °C, with a moisture content of 37–42 %, and sample S3 was collected on day 18. The late stage (S4, days 19–24) saw a decrease in temperature to 40–50 °C and an adjustment in moisture content to 32–37 %, with sample S4 collected on day 24. In the final stage (S5, days 25–30), the center temperature stabilized at 35–45 °C with a moisture content of 30–35 %, and sample S5 was collected on day 30. The fermentation chamber was maintained at 20–30 °C and a relative humidity of 70–80 %. Samples of fermented tea were collected from five distinct locations within the tea pile, homogenized, and rapidly transported to the laboratory, where they were stored at −80 °C for subsequent analysis.

2.3. Calculation of moisture content and required water volume

Moisture content was determined according to GB 5009.3-2016, established by the China National Institute of Standardization (CNIS). The calculations of moisture content and required water volume are as follows:

$$MC\ (\%) = \frac{M_1 - M_2}{M_1 - M_0} \times 100$$

$$\mathrm{WV\_A}_i\ (L) = (m - i \times \mathrm{m}_i) \times \left(\mathrm{WC}_i - \mathrm{WC\_B}_i\right)$$

The parameters in the equations are defined as follows: MC represents the moisture content (%); M_0 is the mass of the weighing bottle (g); M_1 is the mass of the weighing bottle and tea sample before drying (g); M_2 is the mass of the weighing bottle and tea sample after drying (g); WV_A represents the required water volume (L); WC is the target moisture content (%); m represents the initial mass of the tea pile; i is the sampling index, corresponding to the i^{th} sampling event; m_i is the mass of the tea sample taken during the i^{th} sampling event (kg); WC_B is the moisture content before water addition (%).

2.4. Sensory evaluation

2.4.1. Traditional sensory evaluation

The tea was prepared according to the brewing conditions outlined by Li et al. (2019). Specifically, 3 g of tea was infused in 150 mL of boiling water for 5 min, after which the infusion was filtered. The sensory evaluation panel consisted of five professionals with extensive experience in sensory evaluation (three males and two females, aged 23 to 35). The sensory characteristics of the tea were evaluated based on CNIS GB/T 23776–2018, which included evaluation of appearance, liquid color, aroma, taste, and infused leaves. The panelists assessed and scored each sample using a 100-point scale, evaluating the appearance of dried tea leaves, liquid color, aroma, taste, and infused tea leaves. The overall score was determined based on the following weighted criteria: 20 % for appearance, 10 % for liquid color, 25 % for aroma, 35 % for taste, and 10 % for infused leaves.

2.4.2. Colorimeter evaluation

The tea brewing procedure is detailed in Section 2.4.1. A 25-mL tea infusion was placed in a colorimetric cuvette (inner diameter: 10 mm, length: 50 mm). Colorimetric analysis with the colorimeter was performed using HACASuite_V1.00.500 software (Hangzhou Everfine Photo-*E*-Info Co., Ltd). In this analysis, L* (0−100) represents brightness, a* (0–100) and -a* (−100−0) indicate green-redness, respectively, while b* (0–100) and -b* (−100–0) indicate yellow-blueness, respectively.

2.4.3. Electronic tongue evaluation

The method for taste attribute evaluation, as described by Li et al. (2024), was employed in this study. The assessment was performed using an E-tongue system (TS-5000Z, Insent Inc., Atsugi-shi, Japan) equipped with multiple sensor probes: CA0 for sourness, GL1 for sweetness, C00 for bitterness, AE1 for astringency, AAE for umami, and CT0 for saltiness, along with a reference probe.

2.5. Determination of pH

Twenty-five (25) mL of tea infusion were transferred into a centrifuge tube, and the pH was measured using a Mettler Toledo 438 probe.

2.6. Examination of the microscopic structure of tea leaves

The surfaces of the tea samples were examined following the methods of Lin et al. (2024) after a 10-min pretreatment with liquid nitrogen, using SEM (Nova SEM 450, FEI Company, USA (S.E.A.) Pvt. Ltd. Singapore).

2.7. Determination of main chemical components

2.7.1. Determination of cell wall polysaccharides in tea leaves

Cellulose and hemicellulose contents were determined using the methodologies established by Van Soest (1978). Protopectin (PP) content was assessed according to the method described by He et al. (2023). The concentrations of water-soluble pectin (WSP) and total soluble sugars (TSS) were measured using the 3,5-dimethylphenol colorimetric assay and the phenol-sulfuric acid colorimetric assay, respectively (DuBois et al., 1956; Pang et al., 2021). The contents of water extract (WE) and tea polyphenols (TPs) were quantified by the CNIS GB/T 8305–2013 and GB/T 8313–2018, respectively. Soluble protein (SP), total free amino acids (FAAs), and total flavonoids (TFC) were quantified using the Bradford assay, the ninhydrin method, and the aluminum chloride-sodium nitrite method, respectively (Bradford, 1976; Liu et al., 2018; Wang, Li, et al., 2024). *L*-Theanine content was determined following the CNIS GB/T 23193–2017. The concentrations of tea pigments, including theaflavins (TFs), thearubigins (TRs), and theabrownins (TBs), were quantified using a systematic colorimetric method (Ma et al., 2023).

2.7.2. Determination of catechin components, gallic acid, and purine alkaloids

Eight catechin components (C, EC, GC, EGC, CG, ECG, GCG, EGCG), along with GA, CAF, theophylline, and theobromine, were detected using HPLC. Specifically, 0.2 g of uniformly ground tea powder was placed into a 10 mL centrifuge tube. To this, 5 mL of 70 % methanol aqueous solution was preheated to 70 °C. The mixture was stirred thoroughly with a glass rod to ensure uniform wetting and then immediately transferred to a 70 °C water bath for extraction for 10 min, with stirring every 5 min. After extraction, the mixture was cooled to room temperature and centrifuged at 4500 rpm for 15 min. The supernatant was transferred to a 10 mL volumetric flask. The residue was re-extracted with 5 mL of 70 % methanol aqueous solution, and the procedure was repeated. The extracts were combined, diluted to 10 mL, mixed thoroughly, filtered through a 0.22 μm nylon membrane (Jin-Teng, Tianjin, China), and then used for HPLC (Waters 2487, USA) analysis. The chromatographic conditions employed in this study were based on previously reported methods (Cheng et al., 2021) and were suitably modified. Specifically, the chromatographic conditions were as follows: injection volume: 10 μL; UV detection at 278 nm; mobile phase A: acetonitrile; mobile phase B: acetic acid containing ethylene diamine tetraacetic acid; column temperature: 35 °C; flow rate: 1.0 mL/min; gradient elution: 5 % A for 0–5 min, 5–10 % A for 5–20 min, 10–20 % A for 20–25 min, 20–10 % A for 25–35 min, and 10–40 % A for 35–40 min. Total catechin (TC) content was determined following previously reported methods using the formula: TC = GCG + CG + ECG + EGCG + EGC + GC + C + EC (Wang, Liang, et al., 2024).

2.8. Non-targeted metabolomics analysis

Fifty (50) mg of tea sample was added to a 2 mL centrifuge tube, and a 6 mm diameter grinding bead was added. 800 μL of extraction solution (methanol: water = 4:1 (v:v)) containing 0.02 mg/mL of internal standard (L-2-chlorophenylalanine) was used for metabolite extraction. Samples were ground by the Wonbio-96c (Shanghai Wanbo Biotechnology Co., LTD) frozen tissue grinder for 6 min (−10 °C, 50 Hz), followed by low-temperature ultrasonic extraction for 30 min (5 °C, 40 kHz). The samples were left at −20 °C for 30 min, centrifuged for 15 min (4 °C, 13,000g), and the supernatant was transferred to the injection vial for liquid chromatograph mass spectrometer (LC-MS/MS) analysis. A pooled quality control (QC) sample was prepared by mixing equal volumes of all samples. The QC samples were disposed of and tested in the same manner as the analytical samples.

The LC-MS/MS analysis of the sample was performed on a Thermo UHPLC-Q Exactive HF-X system equipped with an ACQUITY HSS T3 column (100 mm × 2.1 mm i.d., 1.8 μm; Waters, USA) at Majorbio Bio-Pharm Technology Co. Ltd. (Shanghai, China). The mobile phases consisted of 0.1 % formic acid in water: acetonitrile (95:5, v/v) (solvent A) and 0.1 % formic acid in acetonitrile: isopropanol: water (47.5:47.5:5, v/v/v) (solvent B). The flow rate and column temperature were set at 0.40 mL/min and 40 °C, respectively.

The mass spectrometric data were collected using a Thermo UHPLC-Q Exactive HF-X Mass Spectrometer, equipped with an electrospray ionization (ESI) source operating in positive and negative modes. The optimal conditions were as follows: source temperature set to 425 °C; sheath gas flow rate at 50 arb; aux gas flow rate at 13 arb; ion-spray voltage floating (ISVF) at -3500 V in negative mode and 3500 V in positive mode; and normalized collision energy of 20–40–60 V for MS/MS. The full MS resolution was set to 60,000, while the MS/MS resolution was 7500. Data acquisition was performed in Data Dependent Acquisition (DDA) mode. The detection was carried out over a mass range of 70–1050 *m/z*. Data were processed in Progenesis QI (Waters Corporation, Milford, USA) for peak identification and alignment, and metabolites were identified using HMDB (http://www.hmdb.ca/) and Metlin (https://metlin.scripps.edu/) databases. The data matrix was uploaded to the Meiji Bio cloud platform (https://cloud.majorbio.com) for further analysis.

2.9. Metagenomics analysis

Metagenomic analysis was performed according to the method reported by He et al. (2023), with necessary modifications. Briefly, 25 g of fermented tea sample was mixed with 125 mL of sterile water and incubated at 120 rpm for 15 min. The mixture was then filtered through four layers of sterile gauze and centrifuged at 4500 rpm for 10 min at 4 °C. The microbial pellet was collected and immediately stored at −80 °C.

Total genomic DNA for metagenomic analysis was extracted from microbial pellets using the FastPure Soil DNA Isolation Kit (Magnetic bead) (MJYH, shanghai, China) following the manufacturer's instructions. The concentration and purity of the extracted DNA were measured using a Synergy HTX microplate reader and a NanoDrop 2000 spectrophotometer, respectively. DNA quality was assessed by electrophoresis on a 1 % agarose gel. The extracted DNA was fragmented to an average size of ~350 bp using the Covaris M220 (Gene Company Limited, China) for paired-end library construction. The paired-end library was prepared using the NEXTFLEX™ Rapid DNA-Seq Kit (Bioo Scientific, Austin, TX, USA). Sequencing was performed on an Illumina NovaSeq™ X Plus platform (Illumina Inc., San Diego, CA, USA) at Majorbio Bio-Pharm Technology Co., Ltd. (Shanghai, China) using the NovaSeq X Series 25B Reagent Kit, following the manufacturer's instructions. Raw sequencing reads were processed using Fastp (version 0.20.0, https://github.com/OpenGene/fastp), where adapter sequences were trimmed, and low-quality reads (length < 50 bp or average quality score < 20) were removed. High-quality reads were assembled using MEGAHIT (version 1.1.2, https://github.com/voutcn/megahit). Contigs ≥300 bp were retained for further analysis. Open reading frames (ORFs) were predicted using Prodigal (version 2.6.3, https://github.com/hyattpd/Prodigal), and ORFs ≥100 bp were extracted. A non-redundant gene catalog was generated using CD-HIT (version 4.7, http://weizhongli-lab.org/cd-hit/) with a sequence identity threshold of 90 % and a minimum coverage of 90 %. Gene abundance in each sample was estimated using SOAPaligner (version 2.21, https://github.com/ShujiaHuang/SOAPaligner) with a 95 % identity threshold. Taxonomic annotation of non-redundant genes was performed by aligning them against the NCBI NR database using DIAMOND (version 2.0.13, http://ab.inf.uni-tuebingen.de/software/diamond/) with an e-value cutoff of 1e-5. Functional annotation was done using DIAMOND against the KEGG, eggNOG, and CAZy databases (Buchfink et al., 2015).

2.10. Statistical analysis

All tests were performed in triplicate, presenting the results as mean ± standard error. One-way analysis of variance (ANOVA) was conducted using IBM SPSS Statistics 27.0 (IBMCorp., Armonk, N.Y., USA). PCA, Partial least squares discriminant analysis (PLS-DA), Orthogonal PLS-DA, PLS regression, and O2PLS were established using SIMCA 14.1 software (Umetrics, Sweden). Differential metabolites were identified based on the criteria of variable importance in projection (VIP > 1), fold change (FC ≥ 2 or ≤ 0.5), and statistical significance ($P < 0.05$). Correlation networks were constructed using Cytoscape 3.9.1 software. Bar charts, bubble charts, and heatmaps were generated using Origin Pro 2024 Student Version (Northampton, USA).

3. Results and discussion

3.1. Analysis of sensory characteristics

The sensory characteristics of sun-dried green tea changed significantly during fermentation (Fig. 1A and Supplementary Table S1). The initial tea sample (S0) had a bright apricot-yellow liquor with a honey-fruity aroma and a grassy, astringent taste. Sample S1 exhibited pronounced sourness and astringency. As fermentation progressed, samples S2 and S3 gradually reduced sourness and astringency, with increased mellowness and higher sensory scores. Sample S4, with a reddish-brown appearance and auburn-red infusion, achieved the highest sensory score (94.0, $P < 0.05$) and was designated MT_RPT. In contrast, sample S5, with a darkened liquor and reduced mellowness, showed slight bitterness and a significant decline in sensory scores (81.4, $P < 0.05$). These results highlight the importance of fermentation degree in shaping RPT flavor, where over-fermentation leads to degradation. Objective analyses using a colorimeter and electronic tongue revealed a significant decrease in brightness (L*), an increase in redness (a*), and a fluctuation in yellowness (b*), which initially rose and then fell ($P < 0.05$, Fig. 1B). Additionally, taste attributes, including sourness, sweetness, bitterness, astringency, umami, saltiness, astringent aftertaste (aftertaste-A), and bitter aftertaste (aftertaste-B), varied across fermentation stages ($P < 0.05$, Fig. 1C).

This study further investigated the impact of sensory attributes on the flavor formation and degradation of MT_RPT using PLS-DA and OPLS-DA models for samples S0–S4 and S4–S5, respectively. PLS-DA analysis revealed that, except for aftertaste-B, all other sensory attributes significantly impacted the flavor formation of MT_RPT (Fig. S2A). Notably, during fermentation, the response values for umami and sweetness remained consistently higher than those for other taste attributes and were significantly correlated with them (Figs. S2B and S2C). These results suggest that these sensory attributes interact to shape the distinctive flavor of MT_RPT. OPLS-DA analysis indicated that increases in the response values for a*, bitterness, and umami, along with decreases in L*, b*, sourness, saltiness, and aftertaste-B, contributed to the

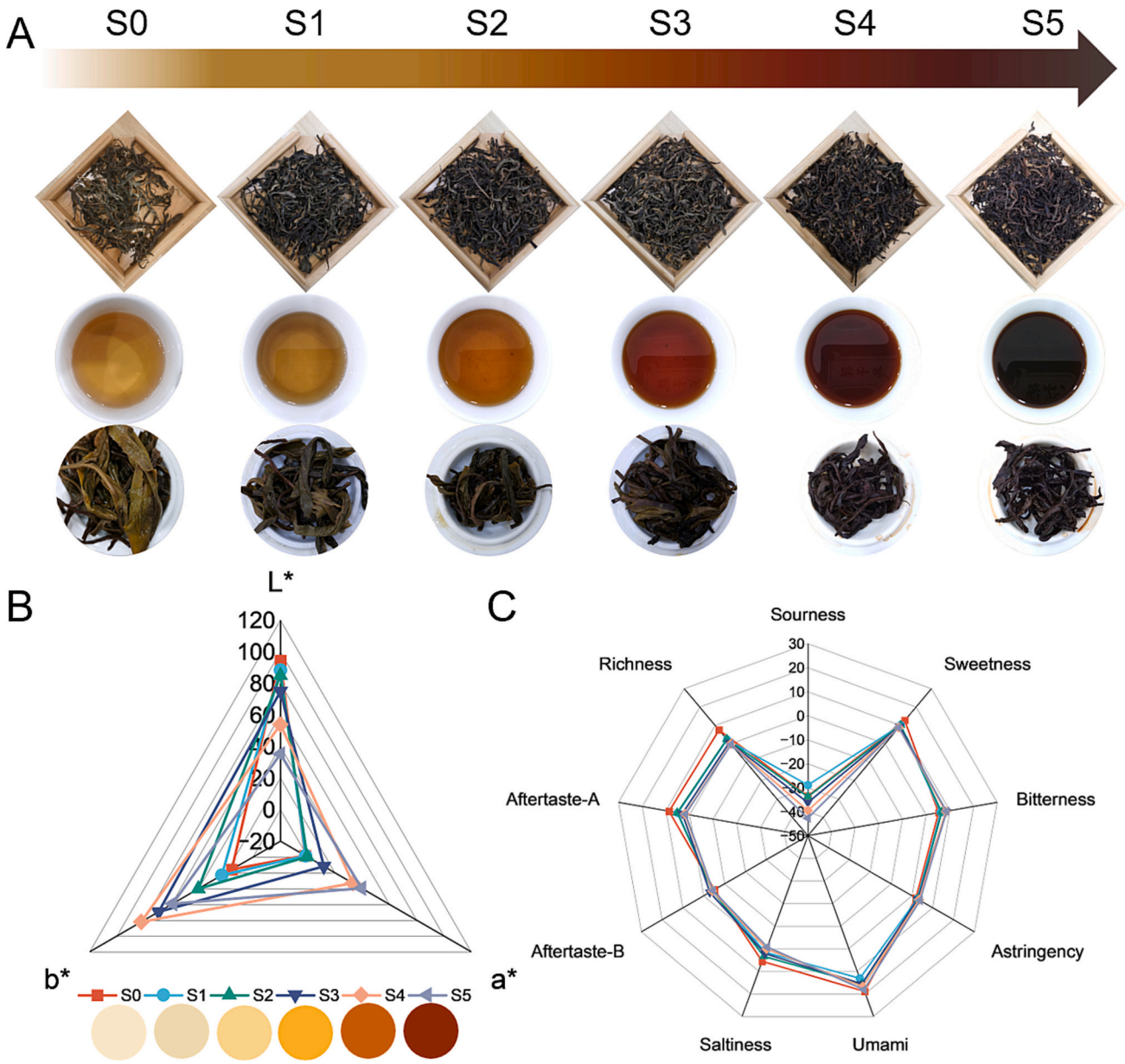

Fig. 1. Sensory changes in tea samples. (A) Visualization of the appearance of dried tea leaves, liquid color, and infused leaves; (B) and (C) Spiderweb plots of liquid color and taste attributes, respectively.

flavor degradation of MT_RPT (Fig. S2D). Additionally, SEM observations revealed that the microstructure of the initial tea leaves was intact, but as fermentation progressed, the structure was disrupted, leading to the curling of the fermented tea leaves (Fig. S2E). These microstructural changes significantly influenced the sensory characteristics and the release of chemical components from the leaves (Pang et al., 2021). In conclusion, these sensory changes provide valuable insights into the flavor formation process of MT_RPT.

3.2. Analysis of the main chemical components

The variation in sensory characteristics of tea is widely recognized to be closely linked to changes in its chemical composition (He et al., 2023; Wang et al., 2023). In this study, 27 main chemical components were quantified, including cellulose, hemicellulose, PP, WSP, WE, TSS, SP, FAAs, *L*-theanine, TPs, TFC, GA, TC, eight catechins, three purine alkaloids, and three types of tea pigments. Polysaccharides in tea cell walls, including cellulose, hemicellulose, and pectin, are critical to the structure and function of the tea (He et al., 2023; Pang et al., 2021). Cellulose levels increased from 137.67 mg/g in S0 to 188.35 mg/g in S5 ($P < 0.05$), hemicellulose showed a slight decrease from 76.86 mg/g in S0 to 74.69 mg/g in S5 (Fig. 2A). These findings are consistent with those of Wang et al. (1991), who observed that hemicellulose remained stable during traditional fermentation. The PP decreased significantly from 22.93 mg/g in S0 to 3.64 mg/g in S5 ($P < 0.05$), and WSP increased from 19.98 mg/g at S0 to 36.95 mg/g at S1, then decreased to 9.49 mg/g at S5 ($P < 0.05$, Fig. 2A). The reduction in PP likely contributed to leaf instability, potentially leading to the curling observed in sensory evaluations. WSP significantly affects the mellowness and thickness of the tea infusion (Deng et al., 2022). The increase in WSP in S4 enhanced the mellowness and thickness of the tea infusion compared to S0, but the decrease in S5 led to a reduction in these flavors.

Water extract (WE) is a standard indicator of tea quality (Li et al., 2017). The WE in S0 was 426.10 mg/g, decreasing in S1, then peaking at 525.83 mg/g in S2 ($P < 0.05$) before decreasing to 500.12 mg/g in S5 (Fig. 2B). This pattern may be attributed to microbes initially consuming

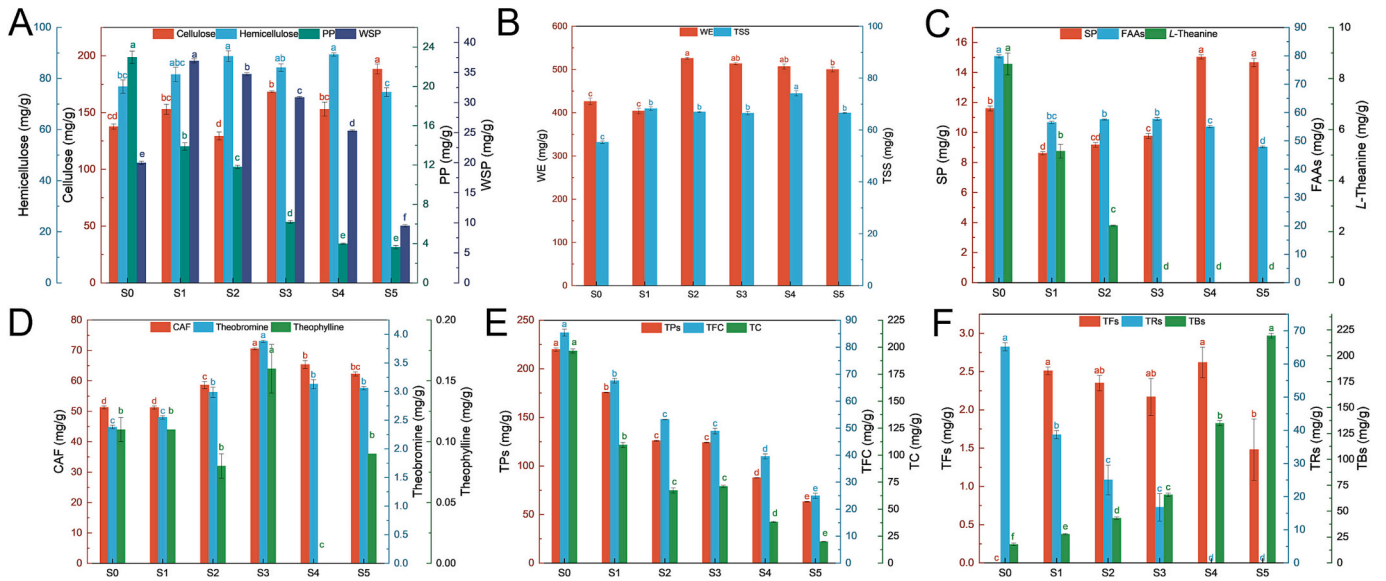

Fig. 2. Changes in the content of the main chemical components. (A) Hemicellulose, cellulose, protopectin (PP), and water-soluble pectin (WSP); (B) Water extract (WE) and total soluble sugars (TSS); (C) Soluble proteins (SP), total free amino acids (FAAs), and *L*-Theanine; (D) Caffeine (CAF), theophylline, and theobromine; (E) Tea polyphenols (TPs), total flavonoids (TFC), and total catechins (TC); (F) Theaflavins (TFs), thearubigins (TRs), and theabrownins (TBs). Statistical significance was determined by Tukey's multiple comparison tests, with significant differences indicated by different letters ($P < 0.05$).

soluble substances, followed by hydrolases releasing insoluble substances from tea leaves. TSS, which is linked to the tea's sweetness and mellowness, rose from 55.27 mg/g in S0 to 74.10 mg/g in S3 before declining to 66.10 mg/g in S5 (Fig. 2B). This trend reflects the degradation of protopectin in tea leaves by pectinase secreted by microbes, which initially increases the TSS content, but subsequent microbial consumption leads to a reduction in its concentration (Deng et al., 2024). SP content decreased from 11.60 mg/g in S0 to 8.62 mg/g in S1, then increased to 14.66 mg/g in S5 (Fig. 2C). FAAs, which influence tea's bitterness, umami, and sweetness (Wang, Li, et al., 2024; Zhang et al., 2023), decreased from 31.93 mg/g in S0 to 19.15 mg/g in S5 (Fig. 2C). *L*-Theanine is a key free amino acid responsible for imparting umami, which significantly decreases after fermentation (Fig. 2C), likely due to microbial consumption or involvement in the synthesis of TBs (Long et al., 2020). CAF, a major bitter component (Wang et al., 2021; Zhang et al., 2023), fluctuated but remained high, increasing from 51.28 mg/g in S0 to 70.73 mg/g in S3, then decreasing to 62.31 mg/g in S5 (Fig. 2D). Theobromine followed a similar trend, peaking at 3.88 mg/g in S3, while theophylline exhibited variation, reaching 0.16 mg/g in S2 and falling below 0.1 mg/g in S4–S5 (Fig. 2D).

TPs significantly influence the bitterness and astringency of tea infusions (Ye et al., 2022). The TPs content reduced considerably from 220.23 mg/g in S0 to 63.21 mg/g in S5 ($P < 0.05$, Fig. 2E). The trend of TFC content mirrored that of TPs (Fig. 2E). Catechins are the primary contributors to astringency in tea infusions (Cao et al., 2019; Li, Lu, et al., 2022). TC showed a significant decrease after fermentation ($P < 0.05$, Fig. 2E). Eight catechins exhibited three patterns: GCG, ECG, and EGCG decreased; C decreased, then increased; EGC, CG, and GC increased, then decreased (Supplementary Table S2). GA, an indicator of fermentation degree in RPT (Li, Lu, et al., 2022), rose from 6.72 mg/g in S0 to 9.83 mg/g in S1 before falling to 0.29 mg/g in S5 (Supplementary Table S2). This change could be attributed to the decomposition of catechins, particularly EGCG, into EGC and GA by tannase, which elevates GA (Xiao et al., 2023). The decrease in GA may also be due to microbial degradation or its involvement in synthesizing TBs (Cao et al., 2018; Hu et al., 2022). Tea pigments are crucial for the liquid color of fermented tea (Hu et al., 2024). TFs were undetected in S0 but increased significantly to 2.51 mg/g in S1 and reached a maximum of 2.62 mg/g in S4 before decreasing to 1.48 mg/g in S5 (Fig. 2F). The increase in TFs is likely attributed to the progressive oxidation of catechins during fermentation (Li et al., 2018). The content of TRs decreased significantly from 65.18 mg/g in S0 to 16.77 mg/g in S2 and was undetected in S4 and S5 (Fig. 2F). This reduction in TRs is likely due to their conversion into TBs during fermentation (Zhu et al., 2020). The TBs content increased significantly from 12.19 mg/g in S0 to 134.84 mg/g in S4 and 219.33 mg/g in S5 ($P < 0.05$, Fig. 2F). This substantial increase in TBs can be attributed to the continuous oxidation and polymerization of catechins and their derivatives (Zhu et al., 2020).

In summary, the contents of WE, TSS, WSP, SP, CAF, theobromine, catechin components (EC and CG), TFs, and TBs were significantly higher ($P < 0.05$) in S4 compared to S0, whereas FAAs, *L*-theanine, theophylline, TPs, TFC, TC, the remaining six catechin components, GA, and TRs were significantly lower ($P < 0.05$). These changes in chemical components are likely crucial in the flavor formation of MT_RPT. Compared to S4, the levels of TSS, WSP, FAAs, TPs, TFC, TC, TFs, GA, and catechin components (C, EC, EGC, CG, ECG, EGCG) were significantly lower ($P < 0.05$) in S5, while the contents of theophylline and TBs were substantially higher ($P < 0.05$). These alterations in chemical composition are likely key factors contributing to the flavor degradation of MT_RPT.

3.3. Analysis of the nonvolatile metabolites

3.3.1. Overall changes in nonvolatile metabolites

This study conducted a relative quantification analysis of nonvolatile metabolites to comprehensively investigate the chemical changes associated with flavor formation in MT_RPT (He et al., 2023). During fermentation, the number of nonvolatile metabolites increased significantly from 4204 at S0 to 4944 at S3 before subsequently declining (Fig. 3A). This pattern suggests that both microbial activity and the humid thermal environment are critical factors influencing the levels of nonvolatile metabolites. A total of 5121 nonvolatile metabolites were identified across all groups, including phenylpropanoids and polyketides (831–959), lipids and lipid-like molecules (734–835), organic acids and derivatives (636–765), organoheterocyclic compounds (626–753), organic oxygen compounds (483–580), benzenoids (388–477), and nucleosides, nucleotides, and analogues (129–159). Notably, all these metabolite classes exhibited a high relative abundance

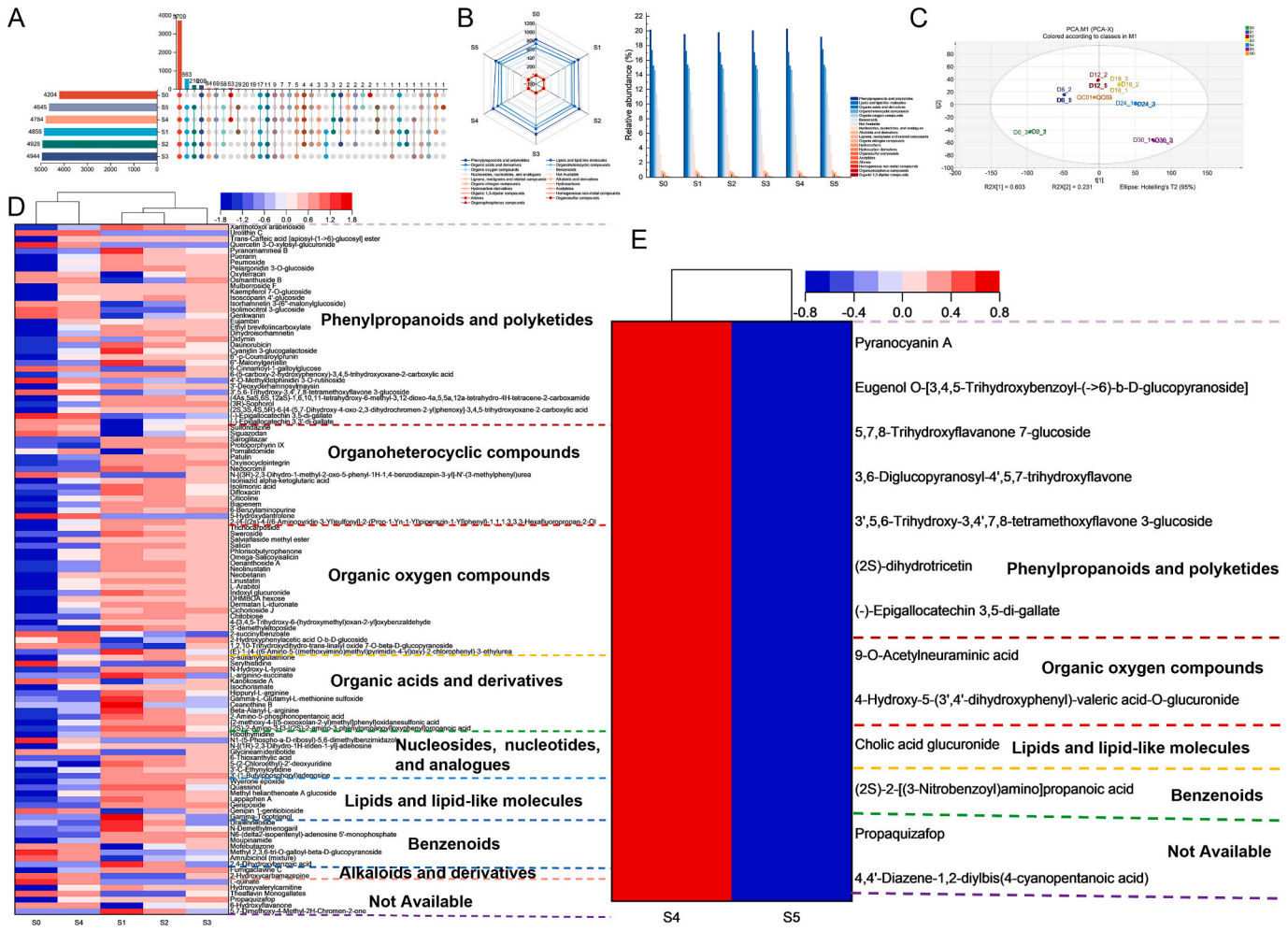

Fig. 3. Changes in nonvolatile metabolites and differential metabolites screening. (A) Changes in the number of nonvolatile metabolites; (B) Changes in the number and relative abundance of differently categorized nonvolatile metabolites; (C) Principal component analysis score plots; (D) Differential metabolite clustering heatmap in S1vsS0, S2vsS0, S3vsS0, S4vsS0, S4vsS1, S3vsS1, S4vsS1, S3vsS2, S4vsS2, and S4vsS3; (E) Differential metabolite clustering heatmap in S4vsS5.

(>3 %) throughout fermentation, underscoring their essential role in MT_RPT flavor formation (Fig. 3B).

3.3.2. *Differential metabolite screening*

The PCA analysis revealed that PC1 and PC2 accounted for 60.3 % and 23.1 % of the variance, respectively, explaining a total of 83.4 % of the data variability (Fig. 3C). These results indicate that the two PC effectively capture the major differences between the samples, highlighting significant variations in the metabolite profiles of tea samples at different fermentation stages. To explore this further, a pairwise comparison of the S0 to S4 samples was performed, and an OPLS-DA model was developed to identify differential metabolites (VIP $>$ 1, P $<$ 0.05, FC $\geq$ 2, or $\leq$ 0.5). The analysis revealed that as fermentation progressed, the metabolite profiles of the tea underwent significant changes. Compared to S0, differential metabolites progressively increased in S1, S2, S3, and S4, with 27, 60, 82, and 100 metabolites identified, respectively (Supplementary Table S3). This indicates substantial changes in both the composition and concentration of metabolites during fermentation. When compared to the previous stage, the number of differential metabolites gradually decreased from S1 to S4, with 17, 28, and 49 metabolites between S1 and S2, S3, and S4; 6 and 18 metabolites between S2 and S3, S4; and 5 metabolites between S3 and S4. This suggests that the fermentation process stabilizes in the later stages, with a reduced magnitude of metabolite changes. A total of 117 statistically significant differential metabolites were identified through pairwise comparisons from S0 to S4, including kaempferol 7-O-glucoside, (−)-epigallocatechin 3,3′-di-gallate, and dihydroisorhamnetin (Fig. 3D). These metabolites comprised 34 phenylpropanoids and polyketides, 22 organic oxygen compounds, 17 organoheterocyclic compounds, 13 organic acids and derivatives, 8 benzenoids, 8 nucleosides, nucleotides, and analogues, 7 lipids and lipid-like molecules, 2 alkaloids and derivatives, and 2 unidentified compounds. Overall, the changes in metabolites during fermentation reflect the progression of biochemical reactions and may also be closely related to the tea's final flavor. Using the same criteria (VIP $>$ 1, P $<$ 0.05, and FC $\geq$ 2 or $\leq$ 0.5), 13 differential metabolites were identified in the comparison between S4 and S5 (Fig. 3E). These metabolites included 7 phenylpropanoids and polyketides—such as (−)-epigallocatechin 3,5-di-gallate, 5,7,8-trihydroxyflavanone 7-glucoside, and 3,6-diglucopyranosyl-4′,5,7-trihydroxyflavone—2 organic oxygen compounds, 1 benzenoid, and 1 lipid or lipid-like molecule.

3.4. *Analysis of microbial community succession*

3.4.1. *Diversity and composition of microbial community*

The microbial community plays a pivotal role in shaping the flavor of RPT by influencing changes in its chemical composition (Wang et al., 2023). α- Diversity, a key indicator of microbial community richness and evenness, is an essential measure of microbial variation (Cheng et al., 2024). Increases in the Chao and ACE indices suggest enhanced species

richness (Fig. S3A), though the slight decline toward the end of fermentation may indicate a reduction in particular species or intensified competition. The increase in the Shannon index reflects greater community diversity, while the decrease in the Simpson index suggests initial unevenness, which later stabilized, implying improved evenness over time. These changes demonstrate the microbial community's adaptation to the fermentation environment, ultimately reaching a stable state. β-Diversity, which highlights compositional differences across fermentation stages, revealed significant shifts in community composition ($P < 0.05$), with the most pronounced differences occurring during mid-fermentation, when the β-diversity index peaked. This suggests a distinct community structure at this stage (Fig. S3B), likely driven by environmental changes and microbial interactions. PCoA further confirmed high similarity within groups and significant differences between groups (Fig. 4A), underscoring the critical role of environmental factors in shaping the microbial community structure throughout fermentation.

The relative abundance of bacteria initially decreased before increasing. In contrast, eukaryotes showed the opposite trend (Fig. 4B). Bacteria consistently maintained a higher relative abundance than eukaryotes, indicating their dominance during the fermentation process and their potential role in shaping the flavor profiles of the product. Based on these findings, this study hypothesizes that bacteria are likely the principal functional microbes responsible for the formation of MT_RPT flavor. At the phylum level, 90 distinct microbial phyla were identified (Fig. 4C). Proteobacteria predominated in the early fermentation stages, with relative abundances of 98.64 % in S0 and 81.02 % in S1, followed by a notable decline. In contrast, Ascomycota and Mucoromycota showed relatively lower abundances of 15.19 % and 2.50 % in S1, respectively, but these increased significantly to 36.19 % and 10.15 % in S2 before decreasing. The relative abundances of Firmicutes and Actinobacteria were 10.29 % and 26.10 % in S2, with these phyla continuing to rise to 46.53 % and 42.03 % in S4, respectively. In S5, Firmicutes abundance decreased to 29.53 %, whereas Actinobacteria abundance surged to 65.60 %. These observations suggest that Proteobacteria dominated the early fermentation stages, Ascomycota and Mucoromycota played significant roles in the early to middle stages, and Firmicutes and Actinobacteria exhibited increased competitiveness in the middle to late stages, ultimately prevailing by the end of fermentation.

At the genus level, 2401 distinct microbial genera were identified (Fig. 4D). In S0, the genera with the highest relative abundances were *Pantoea*, *Klebsiella*, and *Pseudomonas*, with relative abundances of 72.98 %, 9.01 %, and 4.48 %, respectively. In S1, the relative abundances of these genera decreased to 59.58 %, 6.05 %, and 3.76 %, respectively, while the abundance of *Aspergillus* notably increased to 14.73 %. In S2, the relative abundances of *Pantoea* and *Klebsiella* further decreased to 5.37 % and 7.16 %, respectively, and *Aspergillus* abundance rose significantly to 34.48 %. Concurrently, the relative abundances of *Brachybacterium* and *Staphylococcus* increased to 20.08 % and 8.55 %, respectively. In S3, the relative abundance of *Aspergillus* decreased to 17.19 %, while the relative abundances of *Brachybacterium* and *Staphylococcus* increased to 21.52 % and 23.16 %, respectively, and those of *Enterococcus* and *Rothia* rose to 5.65 % and 4.58 %, respectively. In S4, the relative abundance of *Aspergillus* continued to decrease to 3.67 %, while the relative abundances of *Brachybacterium*, *Staphylococcus*, and *Brevibacterium* increased to 24.59 %, 30.58 %, and 6.43 %, respectively. The relative abundances of *Enterococcus* and *Rothia* marginally

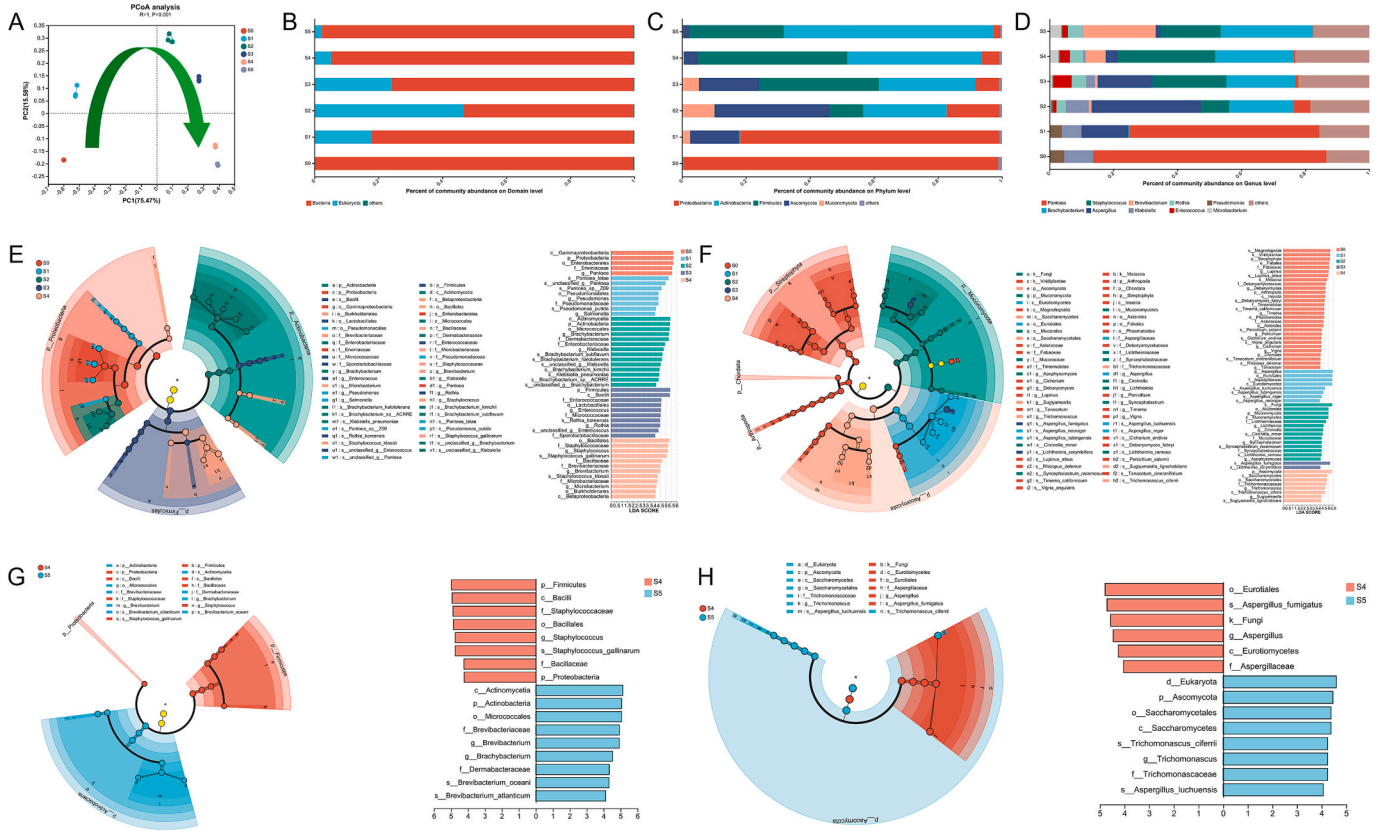

Fig. 4. Diversity and composition of microbial community and microbiomarkers of their succession. (A) Principal coordinate analysis (PCoA) of microbial community variability; (B–D) Microbial community composition at the domain, phylum, and genus levels, respectively, with relative abundance <3 % as "other"; (E) and (F) Pairwise comparison of the microbial communities from S0 to S4 at the bacterial and fungal levels, with microbiomarkers selected based on a linear discriminant analysis (LDA) score > 4, respectively; (G) and (H) Pairwise comparison of the microbial communities from S4 to S5 at the bacterial and fungal levels, with microbiomarkers selected based on an LDA score > 4, respectively.

decreased to 3.03 % and 4.14 %, respectively. In S5, the relative abundances of *Brachybacterium*, *Brevibacterium*, *Rothia*, and *Microbacterium* increased to 28.80 %, 22.86 %, 4.55 %, and 3.67 %, respectively, while the relative abundance of *Staphylococcus* decreased to 18.80 %.

At the species level, 11,082 distinct microbial species were identified (Fig. S3C). Among these, the species with the highest relative abundances in S0 were *Pantoea latae* (34.27 %), *unclassified Pantoea* (17.29 %), *Pantoea* sp.*Z09* (7.48 %), *Klebsiella pneumoniae* (4.05 %), and *unclassified Klebsiella* (3.98 %). In S1, *Pantoea latae* (29.04 %) and *unclassified Pantoea* (14.26 %) retained their dominance, with the emergence of *Aspergillus fumigatus* (4.35 %). In S2, *Aspergillus fumigatus* (11.31 %) became the predominant species, followed by *Staphylococcus gallinarum* (7.20 %) and *Aspergillus luchuensis* (5.77 %). In S3, *Staphylococcus gallinarum* (18.68 %) was the dominant species, accompanied by increased abundances of *Brachybacterium subflavum* (6.27 %) and *Rothia koreensis* (4.53 %). In S5, *Staphylococcus gallinarum* (13.75 %), along with various species of *Brachybacterium* (*Brachybacterium subflavum*, *Brachybacterium halotolerans*, and *Brevibacterium oceani*), were dominant.

In summary, during the early stages of fermentation (0–6 days), Proteobacteria was the predominant phylum, with *Pantoea* as the principal genus and *Pantoea latae* as the dominant species. During the mid-fermentation stage (7–12 days), the *Aspergillus*, particularly *Aspergillus fumigatus*, exhibited a significant increase in abundance, becoming the dominant microbe. In the mid-late stage (13–18 days), *Aspergillus*, *Brachybacterium,* and *Staphylococcus* became prominent, with the abundance of *Staphylococcus gallinarum* notably increasing. Finally, in the late and final stages (19–30 days), *Brachybacterium*, *Staphylococcus*, and *Brevibacterium* emerged as the dominant genera. Previous studies have demonstrated that *Aspergillus* is a dominant microorganism in microbial fermentation and commercial RPT (Zhu et al., 2020). In traditional pile fermentation of RPT, *Aspergillus* was dominant in the early stages, but its relative abundance significantly decreased in the late stages of fermentation (Zhang et al., 2013), while *Staphylococcus* increased dramatically during the later stages (Wang et al., 2023). Thus, basket fermentation and traditional pile fermentation share similarities in microbial composition but exhibit notable differences. For instance, Li et al. (2018) discovered that the abundance of eukaryotes was higher during natural pile fermentation, whereas bacteria played a crucial role in the later stages of fermentation. These disparities could result from differences in raw materials, processing techniques, and fermentation conditions, all of which collectively influence the flavor profile of the final fermented tea product (Ge et al., 2021; Li et al., 2018).

3.4.2. Microbiomarkers of community succession

Differences in bacterial and fungal communities were analyzed using linear discriminant analysis effect size (LEfSe), with a threshold of 2.0 for the linear discriminant analysis (LDA) score to identify microbiomarkers exhibiting significant shifts in relative abundance across different fermentation stages (Wang et al., 2023). The results revealed that various microbes, such as *Pantoea*, *Bacillus*, and *Aspergillus*, played essential roles as microbiomarkers during the MT_RPT fermentation process (Figs. S4A and S4B). However, the complexity of microbial communities made identifying the key microbiomarkers responsible for MT_RPT flavor formation challenging. Therefore, this study focused on microbiomarkers with LDA values greater than 4 in bacteria and eukaryotic for subsequent analyses. In S0, *Pantoea* was the predominant bacterial marker (Fig. 4E), while fungal markers included *Penicillium*, *Cichorium*, *Lupinus*, *Timema*, *Vigna*, *Debaryomyces*, *Tanacetum*, and *Rhizopus* (Fig. 4F). In S1, bacterial markers shifted to *Salmonella* and *Pseudomonas*, with *Pantoea* (*Pantoea* sp. Z09 and *Pantoea* latae) still detected. The fungal community transitioned to *Aspergillus* (*Aspergillus luchuensis* and *Aspergillus niger*). In S2, *Klebsiella* and *Brachybacterium* were added to the bacterial markers, while the fungal community was primarily composed of *Lichtheimia*, *Circinella*, *Syncephalastrum*, and *Apophysomyces*. In S3, *Enterococcus* and *Rothia* were the dominant bacterial markers, and the fungal markers included *Aspergillus* and *Lichtheimia*. In S4, bacterial markers consisted mainly of *Staphylococcus*, *Brevibacterium*, and *Microbacterium*, while fungal markers included *Sugiyamaella* and *Trichomonascus*. In S5, *Brevibacterium* was the principal bacterial marker (Fig. 4G), while fungal markers included *Trichomonascus* and *Aspergillus* (Fig. 4H).

3.4.3. Characteristic functions of microbial communities

The analysis of microbial community functions at different fermentation stages provides a deeper understanding of their role in the flavor formation process of MT_RPT (He et al., 2023). COG functional annotation identified “metabolism,” particularly “carbohydrate transport and metabolism,” as the most abundant category (Fig. S5A). At KEGG level 2, the categories “global and overview maps,” “carbohydrate metabolism,” and “amino acid metabolism” also exhibited high abundance (Fig. S5B). Additionally, CAZyme annotations highlighted the dominance of glycoside hydrolases (GHs, Fig. S5C). These findings suggest that the MT_RPT fermentation process is primarily driven by the microbial community’s carbohydrate and amino acid metabolism, with GHs facilitating microbial growth by breaking down complex carbohydrates into energy and nutrients (Bian et al., 2022).

LEfSe analysis identifies characteristic functions and metabolic pathways based on functional gene abundance, enabling the identification of core functional microbial communities across different groups (Zhang, Fan, et al., 2024). Functional shifts from S0 to S4 were evident in the COG, KEGG level 2, and CAZyme analyses. At the COG level, S0 showed functions linked to cell wall/membrane/envelope biogenesis, amino acid transport/metabolism (Fig. S5D), and cell motility, while S2 exhibited functions related to energy production, lipid/carbohydrate metabolism, and transport. S3 was linked to translation and ribosomal biogenesis, and S4 was associated with nucleotide metabolism, replication/repair, and coenzyme transport. At KEGG level 2, S0 featured functions related to membrane transport, cell motility, and prokaryotic communities, while S1 was linked to xenobiotic metabolism (Fig. S5E). S2 focused on transport, catabolism, and protein folding, S3 emphasized signaling molecules, and S4 highlighted carbohydrate, lipid, and amino acid metabolism. CAZyme analysis revealed a dominance of glycosyltransferases (GTs) in S0 (Fig. S5F), GHs, carbohydrate-binding modules (CBMs), polysaccharide lyases (PLs), and auxiliary activities (AAs) in S2, and cellulosome modules (CMs) and carbohydrate esterases (CEs) in S4. Functional shifts in S5 were observed at the COG, KEGG level 2, and CAZyme levels compared to S4. At the COG level, S4 was associated with replication/repair, cell wall/membrane biogenesis, and carbohydrate metabolism, while S5 shifted to energy production, amino acid metabolism, and transcription (Fig. S5G). At KEGG level 2, S4 featured lipid/carbohydrate metabolism and cell motility, while S5 focused on translation, global overview maps, and amino acid metabolism (Fig. S5H). CAZyme analysis showed that S4 exhibited GHs, CBMs, and PLs, while S5 highlighted CEs, AAs, GTs, and CBMs (Fig. S5I).

Overall, microbial functions during fermentation demonstrate distinct stage-specific adaptations. In the early stages (S0 and S1), functions are directed toward environmental acclimation and basic cellular processes, with S0 characterized by cell motility, membrane transport, and cell wall/membrane biogenesis, while S1 focuses on xenobiotic metabolism. These processes facilitate amino acid assimilation for protein synthesis and energy production. The middle stage (S2) marks a metabolic transition, emphasizing energy production, carbon metabolism, transport, and protein folding. In the mid-late and late stages (S3 and S4), functional specialization intensifies, with S3 prioritizing translation and ribosomal biogenesis and S4 focusing on nucleotide metabolism, replication/repair, and the accumulation of essential metabolites such as carbohydrates, lipids, and amino acids. The final stage (S5) involves energy management, amino acid metabolism, transcriptional regulation, and diversified enzymatic activities, reflecting metabolic adjustments in preparation for fermentation completion.

3.5. Identification of key compounds, core functional microbes, and impact factors for MT_RPT flavor formation and degradation process

3.5.1. Association analysis of sensory attributes and differential compounds

To elucidate the compounds underlying MT_RPT flavor formation, a PLS regression model was developed to link 11 sensory attributes with 141 differential compounds, including 24 primary chemical components and 117 differential metabolites across stages S0 to S4 (Ma, Wei, et al., 2024; Mohammadi et al., 2024). The analysis identified 77 compounds as key contributors to MT_RPT flavor formation (VIP > 1, Fig. 5A and Fig. S6A). Further correlation network analysis revealed 49 key flavor compounds (16 chemical components and 33 metabolites) strongly associated with sensory attributes (correlation coefficient $|r| \geq 0.8$, $P < 0.05$, Fig. 5B). Regarding liquid color attributes, *L*-Theanine, TPs, TFC, TRs, TC, and catechin compounds (EC, ECG, EGCG, GCG) were significantly negatively correlated with both a* and b*, while exhibiting a significant positive correlation with L*. In contrast, TBs and didymin were significantly positively correlated with both a* and b*, but negatively correlated with L*. Additionally, GA showed a significant negative correlation with a*, while CAF and theobromine showed a positive correlation with b*. For taste attributes, umami was significantly positively correlated with glycineamide ribotide and isorhamnetin-3-O-(6″-malonylglucoside) but negatively correlated with 28 compounds, including pelargonidin 3-O-glucoside, dihydroisorhamnetin, and puerarin. Sweetness was positively correlated with *L*-Theanine, TPs, catechins (EC, ECG, EGCG, GCG), and TRs but negatively correlated with TBs, theobromine, and didymin. Sourness showed a positive correlation with *L*-Theanine, TFC, and catechins (EC, ECG, EGC, EGCG), but negative correlation with TBs. Bitterness showed a positive correlation with TBs, CAF, theobromine, and didymin but a negative correlation with *L*-Theanine, TPs, TFC, catechins (EC, ECG, EGCG), and TRs. Astringency was positively correlated with DHMBOA hexose, didymin, mulberroside F, and TBs while negatively correlated with *L*-Theanine, TFC, TC, catechins (EC, ECG, EGC, EGCG), TPs, and TRs. Aftertaste-A was positively correlated with *L*-Theanine, TPs, TFC, catechins (EC, ECG, EGCG), and TRs but negatively with TBs. Saltiness exhibited a positive correlation with FAAs and a negative correlation with TSS. Richness was positively correlated with FAAs, *L*-Theanine, TPs, catechins (EC, ECG, EGCG), TFC, and TRs while negatively correlated with TBs.

Based on VIP > 1, $|r| \geq 0.8$, and $P < 0.05$, 24 key compounds were identified as significant contributors to the flavor degradation of MT_RPT (Fig. 5C, D, and S6B). In brief, the a* showed a significant positive correlation with theophylline and TBs, while it was negatively correlated with several compounds, including TFC, catechins (EC, GC, CG, ECG), and seven metabolites such as cholic acid glucuronide, 3′,5,6-trihydroxy-3,4′,7,8-tetramethoxyflavone 3-glucoside, 5,7,8-trihydroxyflavanone 7-glucoside, and (2*S*)-dihydrotricetin. Both L* and b* were positively correlated with WSP, FAAs, TC, catechins (C and EGC), and (−)-epigallocatechin 3,5-di-gallate, 3,6-diglucopyranosyl-4′,5,7-trihydroxyflavone, 9-*O*-acetylneuraminic acid. TFC and five metabolites, including 4-hydroxy-5-(3′,4′-dihydroxyphenyl)-valeric acid-O-glucuronide, were positively correlated with aftertaste-B but negatively correlated with bitterness. Saltiness was positively correlated with TFC, GC, and nine metabolites, including (−)-epigallocatechin 3,5-di-gallate, 3,6-diglucopyranosyl-4′,5,7-trihydroxyflavone, and (2*S*)-2-[(3-

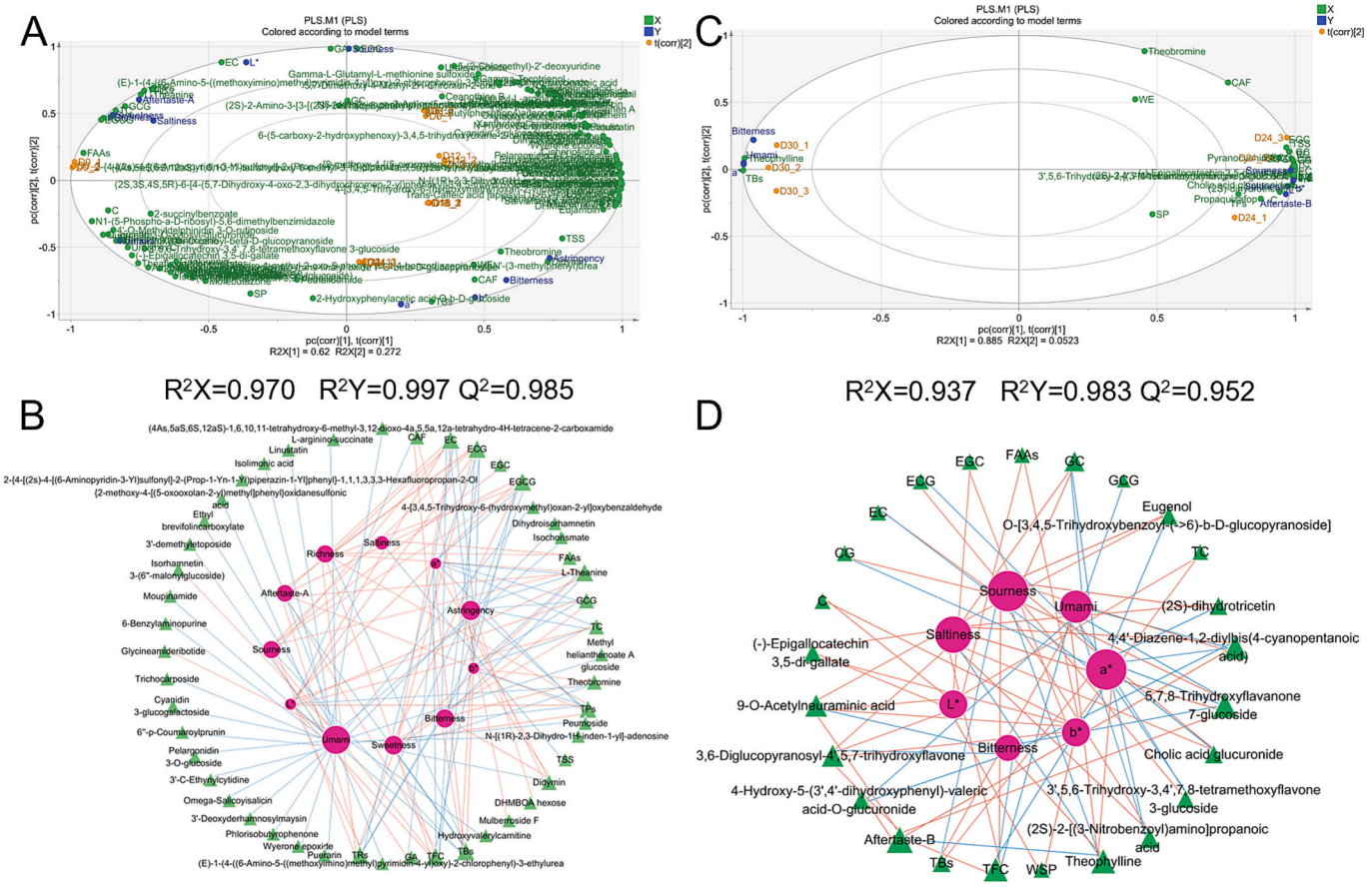

Fig. 5. Association analysis of sensory attributes with differential compounds during the flavor formation and degradation of mellow and thick-type ripened Pu-erh tea (MT_RPT). (A) and (B) Biplot of partial least squares (PLS) regression and correlation network of sensory attributes with differential compounds during the MT_RPT flavor formation process, respectively; (C) and (D) Biplot of PLS regression and correlation network of sensory attributes with differential compounds during the MT_RPT flavor degradation process, respectively.

nitrobenzoyl)amino]propanoic acid. Sourness was positively correlated with TFC, catechins (CG, EC, ECG, GC), and seven metabolites, including 4,4′-diazene-1,2-diylbis(4-cyanopentanoic acid), (2*S*)-dihydrotricetin, and eugenol O-[3,4,5-trihydroxybenzoyl-(→6)-β-D-glucopyranoside], but negatively correlated with TBs. Umami was negatively correlated with TFC, catechins (GC, GCG), and five metabolites, including 5,7,8-trihydroxyflavanone 7-glucoside, but positively correlated with TBs. Additionally, theophylline exhibited a positive correlation with bitterness and umami and a negative correlation with aftertaste-B, saltiness, and sourness.

3.5.2. *Association analysis of microbiomarkers, characteristic functions, and key flavor compounds*

The dynamic changes in flavor compounds during tea fermentation are closely linked to the metabolic activity of microbes (Wang et al., 2023). An O2PLS model was developed to evaluate the influence of 24 microbiomarkers on 49 key flavor compounds in the MT_RPT flavor formation process (Fig. 6A). The results indicated that 11 microbiomarkers were identified as significantly influencing the key flavor compounds (VIP > 1, Fig. S7A). A correlation network established between these 11 microbiomarkers and the 49 key flavor compounds revealed eight microbes with highly significant correlations ($|r| \geq 0.8$ and $P < 0.05$), including *Brachybacterium*, *Lupinus*, *Pantoea*, *Pseudomonas*, *Rothia*, *Salmonella*, *Sugiyamaella*, and *Trichomonascus* (Fig. 6B). Notably, *Pantoea*, *Brachybacterium*, *Rothia*, and *Pseudomonas* exhibited a relative abundance of greater than 5 % among these microbiomarkers, indicating their significant role in the changes of key flavor compounds (Fig. 6C). Additionally, *Aspergillus*, *Staphylococcus*, and *Brevibacterium* were identified as key microbiomarkers significantly affecting the key flavor compounds during the MT_RPT flavor degradation process (VIP > 1, $|r| \geq 0.8$, $P < 0.05$, relative abundance >5 %) (Fig. 6D and E, Figs. S8A and S8B). Notably, the decrease in *Aspergillus* and *Staphylococcus* and the

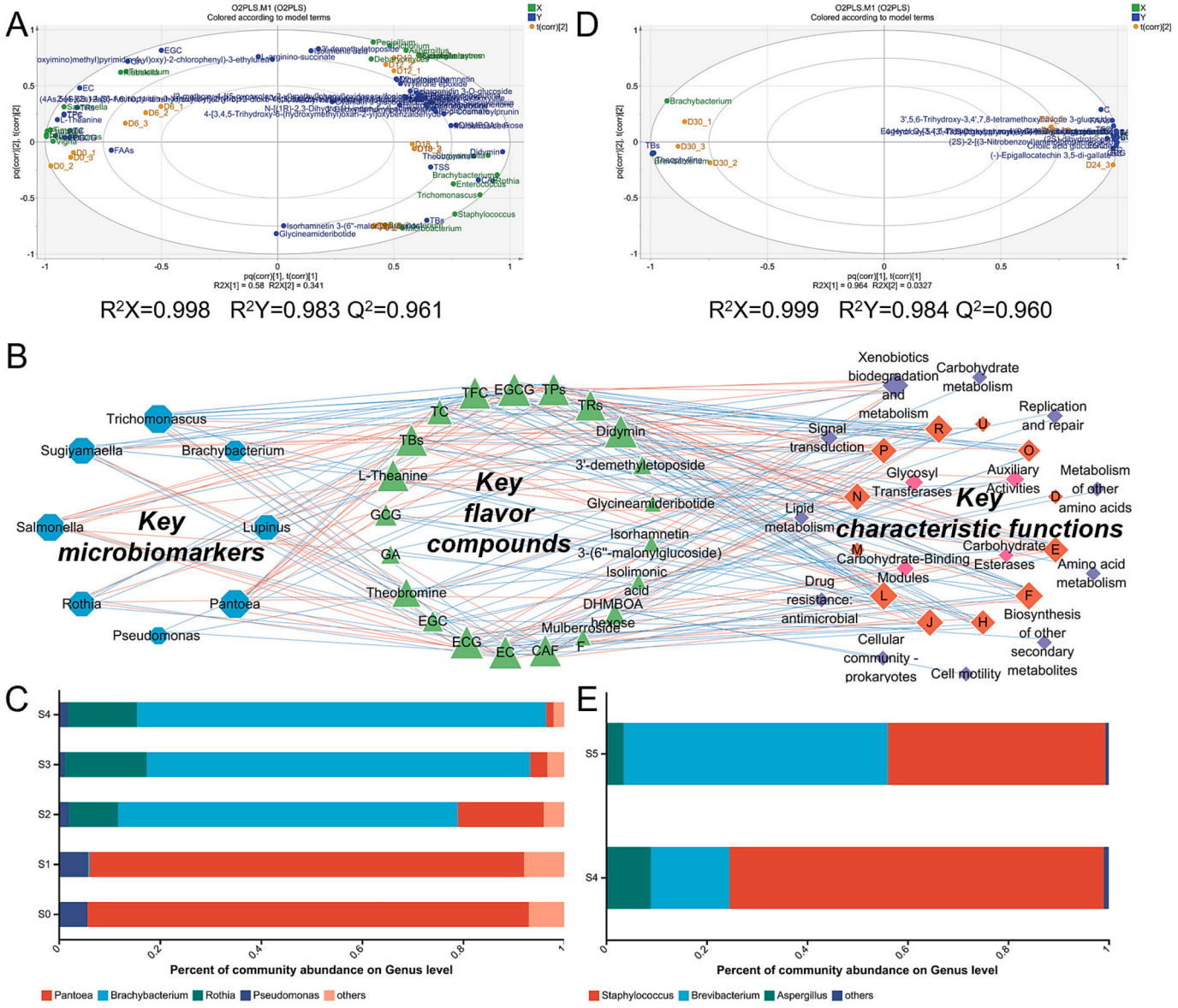

Fig. 6. Association of microbiomarkers, characteristic functions, and key flavor compounds during the flavor formation and degradation of mellow and thick-type ripened Pu-erh tea (MT_RPT). (A) Two-way orthogonal partial least squares (O2PLS) association analysis biplots of microbiomarkers with key flavor compounds during the MT_RPT flavor formation process; (B) Correlation network between microbiomarkers, characteristic functions, and key flavor compounds during the MT_RPT flavor formation process, with $|r| \geq 0.8$ and $P < 0.05$; (C) Relative abundance of key microbiomarkers during the MT_RPT flavor formation process, with relative abundance <5 % as "other"; (D) O2PLS association analysis biplots of microbiomarkers with key flavor compounds during the MT_RPT flavor degradation process; (E) Relative abundance of key microbiomarkers during the MT_RPT flavor degradation process, with relative abundance <5 % as "other."

increase in Brevibacterium characterized the MT_RPT flavor degradation process. Consequently, *Pantoea*, *Pseudomonas*, *Brachybacterium*, *Rothia*, *Aspergillus*, and *Staphylococcus* were identified as key microbiomarkers involved in MT_RPT flavor formation.

Based on VIP > 1, $|r| \geq 0.8$, and $P < 0.05$, categories E, R, J, H, P, M, O, L, F, D, N, and U at the COG functional level were significantly correlated with key flavor compounds during the MT_RPT flavor formation process. At the KEGG level, carbohydrate, amino acid, and lipid metabolism pathways also demonstrated significant correlations with these compounds. At the CAZyme level, GTs, CEs, AAs, and CBMs had notable effects (Fig. 6B, Figs. S7B and S7C). In contrast, during the MT_RPT flavor degradation process, categories G, E, R, K, H, P, I, M, C, L, S, F, X, Q, and D at the COG functional level significantly influenced key flavor compounds (Fig. S8B-S8D). At the KEGG level, pathways such as xenobiotics biodegradation and metabolism and glycan biosynthesis and metabolism exhibited significant associations. At the CAZyme level, GHs, GTs, CEs, and AAs also played essential roles.

3.5.3. *Analysis of the contribution of key microbiomarkers to characteristic functions*

Given that different microbes may share the same function or a single microorganism may possess multiple functions, analyzing the

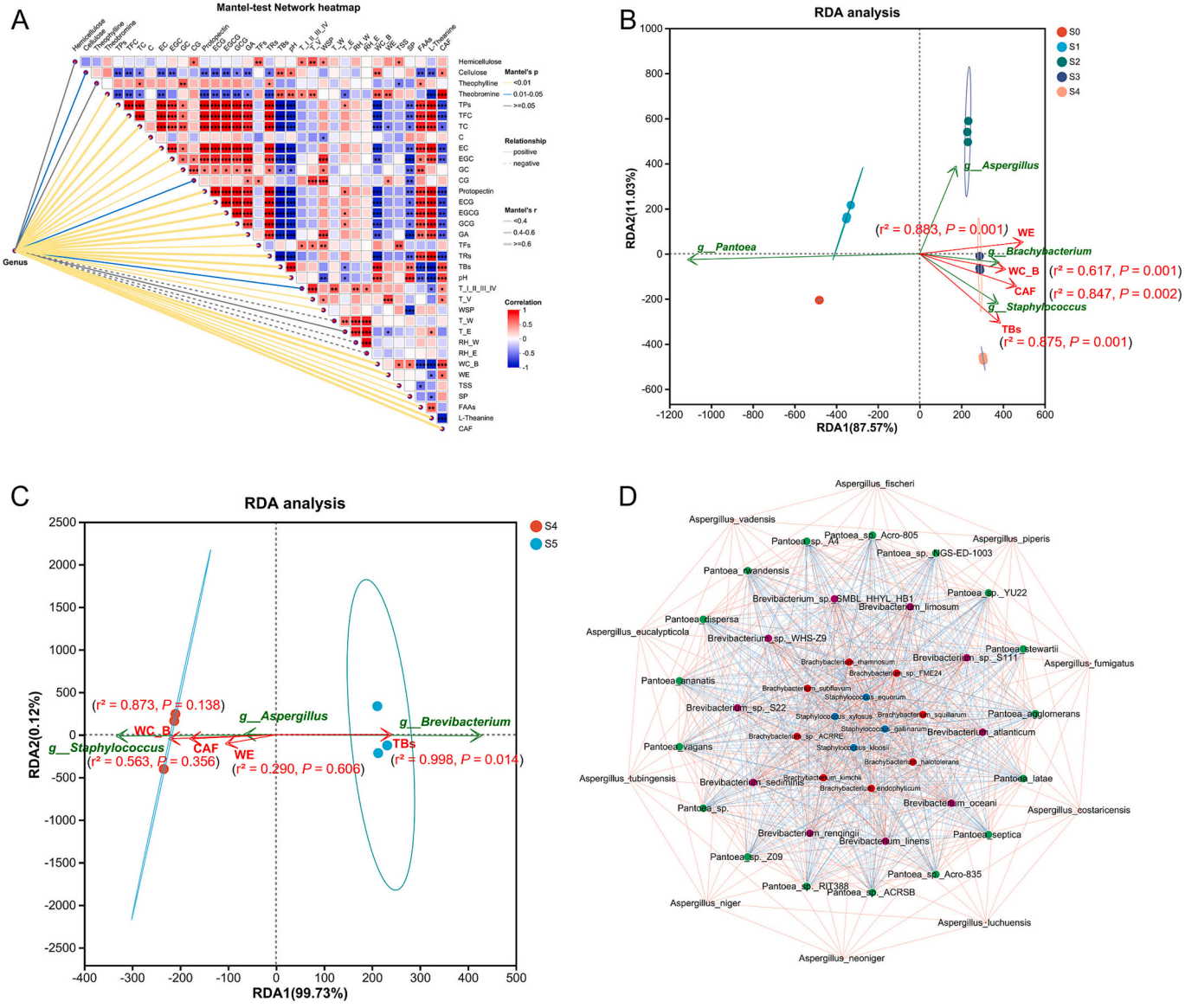

Fig. 7. Association of core functional microbes with fermentation parameters and main chemical components during the flavor formation and degradation of mellow and thick-type ripened Pu-erh tea (MT_RPT). (A) Mantel's test heatmap shows the correlation between core functional microbial communities and fermentation parameters, main chemical components. The lines in the graph represent correlations between microbial communities and environmental factors, with line thickness indicating the strength of the correlation (Mantel's r, absolute value of R). The heatmap displays the correlation between impact factors, with colors representing positive (red) and negative (blue) correlations. Color depth reflects the magnitude of correlations, and asterisks indicate statistical significance: * $0.01 < P \leq 0.05$, ** $0.001 < P \leq 0.01$, *** $P \leq 0.001$. (B) and (C) Redundancy analysis (RDA) of core functional microbes and impact factors during MT_RPT flavor formation and degradation. Dots represent samples, with colors and shapes indicating different subgroups and distances between dots reflecting similarities in functional composition. Red and green arrows represent environmental factors and core functional microbes, respectively, with arrow lengths indicating the correlation strength. Arrow angles indicate the direction of correlation: acute for positive, obtuse for negative, and right angles for no correlation; (D) Interactions among core functional microbes at the species level. Nodes represent microbial species, and edges represent correlations, with red lines indicating positive correlations and blue lines indicating negative correlations; $|r| \geq 0.6$, $P < 0.05$. (For interpretation of the references to color in this figure legend, the reader is referred to the web version of this article.)

contribution of microbes to functional genes is essential for identifying those that significantly contribute to specific functions (Zhu et al., 2019). In the early fermentation stage, *Pantoea* and *Aspergillus* are key microbiomarkers and primary contributors to functional genes (Supplementary Table S4). While *Kalamiella* and *Mixta* also have some influence, their relatively low abundance at this stage makes them less relevant to this study. During the middle to mid-late fermentation stages, *Aspergillus*, *Brachybacterium*, and *Staphylococcus* emerge as the main contributors. In the late fermentation stage, *Brachybacterium* and *Staphylococcus* remain dominant. In the final fermentation stage, *Brevibacterium*, *Aspergillus*, and *Staphylococcus* are the key microbiomarkers and primary contributors to functional genes (Supplementary Table S5).

3.5.4. Association analysis of core functional microbes with fermentation parameters and main chemical components

Temperature, humidity, moisture content, and pH are key fermentation parameters that significantly influence the flavor of tea (Li et al., 2023; Long, Li, et al., 2024). The temperature at the center of the tea pile (T_V, 47.83 °C) was higher than that of the surrounding areas (T_I, T_II, T_III, T_IV, 45.57 °C), primarily due to the center's reduced exposure to external factors and the surrounding area's more rapid heat dissipation (Figs. S9A and S9B). Fermentation temperatures reached their peak during the mid-stage (S2, 48.87 °C) and mid-late stage (S3, 49.58 °C), surpassing those of the early stage (S1, 42.98 °C), late stage (S4, 46.95 °C), and final stage (S5, 41.72 °C), coinciding with periods of intense microbial growth and enzymatic activity. As fermentation progressed, the moisture content in the tea pile gradually decreased, and the rate of water loss slowed as the humidity declined (Fig. S9C), indicating a reduced microbial water demand as fermentation advanced. The pH dropped from 5.65 at S0 to 5.32 at S1 (Fig. S9D) and subsequently increased to 6.97 at S5, reflecting an initial increase in acidity at the onset of fermentation, followed by a gradual decrease corresponding with sensory evaluations.

The flavor of fermented foods is influenced not only by fermentation parameters but also by the main chemical components in the raw materials (Xiong et al., 2024). These components significantly impact food flavor by regulating the succession of microbial communities. In this study, the Mantel test was used to analyze the impact of temperature, humidity, moisture content, pH, and main chemical components on core functional microbial communities (Fig. 7A). The results revealed a highly significant correlation ($|r| \geq 0.6$, $P < 0.01$) between the succession of core functional microbial communities and several factors, including protopectin, WE, *L*-Theanine, CAF, TPs, TFC, TC, catechin compounds (EC, GCG, ECG, EGCG), GA, TRs, TBs, pH, and WC_B. Furthermore, significant autocorrelations were observed among these factors. For example, TPs showed a significant positive correlation with TFC and a significant negative correlation with TBs, while TBs were significantly positively correlated with pH ($P < 0.05$). These findings suggest that these factors influence the assembly and distribution of core functional microbial communities through synergistic or antagonistic interactions. To improve the accuracy of the correlation analysis between influencing factors and core functional microbes, a variance inflation factor (VIF < 5) analysis was performed, eliminating factors with high autocorrelation and selecting the most representative influencing factors (Zhang, Guo, et al., 2024). The screening results indicated that WE, CAF, TBs, and WC_B were significantly associated with core functional microbes (Supplementary Tables S6 and S7).

Redundancy analysis (RDA) further elucidated the interactions between key factors and core functional microbes in the formation of MT_RPT flavor (Liang et al., 2024). The results showed that RDA 1 and RDA 2 accounted for 87.57 % and 11.03 % of the total constrained variation, respectively (Fig. 7C). WE ($r^2 = 0.883$, $P = 0.001$), TBs ($r^2 = 0.875$, $P = 0.001$), CAF ($r^2 = 0.847$, $P = 0.002$), and WC_B ($r^2 = 0.617$, $P = 0.001$) were strongly correlated with the core functional microbial community. Specifically, *Pantoea*, a core functional microbe in the early fermentation stage, showed a significant negative correlation with WE, CAF, TBs, and WC_B. In contrast, *Aspergillus*, a core functional microbe during the mid to mid-late fermentation stages, showed a significant positive correlation with WE. During the mid to late fermentation stages, core functional microbes, including *Brachybacterium* and *Staphylococcus*, exhibited positive correlations with CAF, TBs, and WC_B. Additionally, during the flavor degradation of MT_RPT, TBs ($r^2 = 0.998$, $P = 0.02$) exhibited a significant negative correlation with *Aspergillus* and *Staphylococcus* while exhibiting a significant positive correlation with *Brevibacterium*. Notably, WC_B, WE, CAF, and TBs serve as crucial state indicators reflecting the fermentation process of MT_RPT. Consequently, regulating these indicators necessitates direct adjustment of the relevant parameters. The correlation analysis results indicated that WE is significantly positively correlated with T_V, and both TBs and CAF exhibited significant positive correlations with pH ($P < 0.05$, Fig. 7A). Therefore, WC_B, T_V, and pH are essential fermentation parameters for optimizing the flavor formation process of MT_RPT.

Additionally, the microbiome composition underwent significant changes during fermentation, which likely had a substantial impact on the chemical composition of the tea. To explore microbial interactions and growth-regulatory mechanisms during fermentation, a species-level network was constructed among the core functional microbes (Li et al., 2016; Wang et al., 2023). This network consisted of 49 nodes and 786 edges, of which 412 were positively correlated (Fig. 7D), indicating a significant positive symbiotic relationship among the core microbes ($|r| \geq 0.6$, $P < 0.05$). Such positive correlations are crucial for maintaining microbial community stability and facilitating succession, ensuring continuity and dynamic balance (Liu et al., 2024). Specifically, during MT_RPT flavor formation, *Pantoea* was negatively correlated with *Brachybacterium* and *Staphylococcus*, whereas *Brachybacterium* and *Staphylococcus* showed a positive correlation. In contrast, during MT_RPT flavor degradation, *Aspergillus* and *Staphylococcus* showed a negative correlation with Brevibacterium.

3.6. Flavor formation and degradation processes of MT_RPT

The flavor formation of MT_RPT is a dynamic, multi-stage biochemical process influenced by interactions among fermentation parameters, core functional microbes, characteristic microbial functions, and key flavor components (Li et al., 2023; Ma, Ma, et al., 2024; Wang et al., 2023). During the early fermentation stage (0–6 days), the microbial community primarily adapts to the environment and regulates fundamental cellular processes. The core microbe, *Pantoea*, significantly decreases in abundance. At the same time, *Aspergillus* begins to grow and proliferate (Fig. 8). Despite the decline in *Pantoea* levels, it remains the dominant microbe, contributing to substantial reductions in *L*-Theanine, TFC, catechins (EC, ECG, EGCG), and TRs, while TBs increase. These changes in key flavor compounds collectively enhance the yellow hue (b*), sourness, astringency, and bitterness of the tea infusion, while simultaneously reducing brightness (L*), sweetness, aftertaste-A, and richness. Additionally, 12 key metabolites, including puerarin, phlorisobutyrophenone, and didymin, are significantly upregulated, decreasing umami. FAAs decrease, whereas TSS increases, resulting in reduced saltiness. By the sixth day (S1), the tea infusion appears greenish-yellow and slightly cloudy, with pronounced sourness and astringency.

During the middle-to-mid-late fermentation stage (7–18 days), the microbial community primarily engages in energy production, carbon metabolism, material transport, and protein folding. *Aspergillus* levels increase significantly, while *Brachybacterium* and *Staphylococcus* begin to proliferate. These core functional microbes collectively contribute to significant decreases in TPs, TFC, *L*-Theanine, TC, GA, catechins (EGC, ECG, EGCG, GCG), TRs, 3′-demethyletoposide, and isolimonic acid, while CAF, theobromine, EC, TBs, and glycineamide ribotide increase significantly. These changes in key flavor compounds increase a* and b* and heightened bitterness and umami, while L*, sourness, sweetness, aftertaste-A, and richness decrease. By the 18th day (S3), the tea

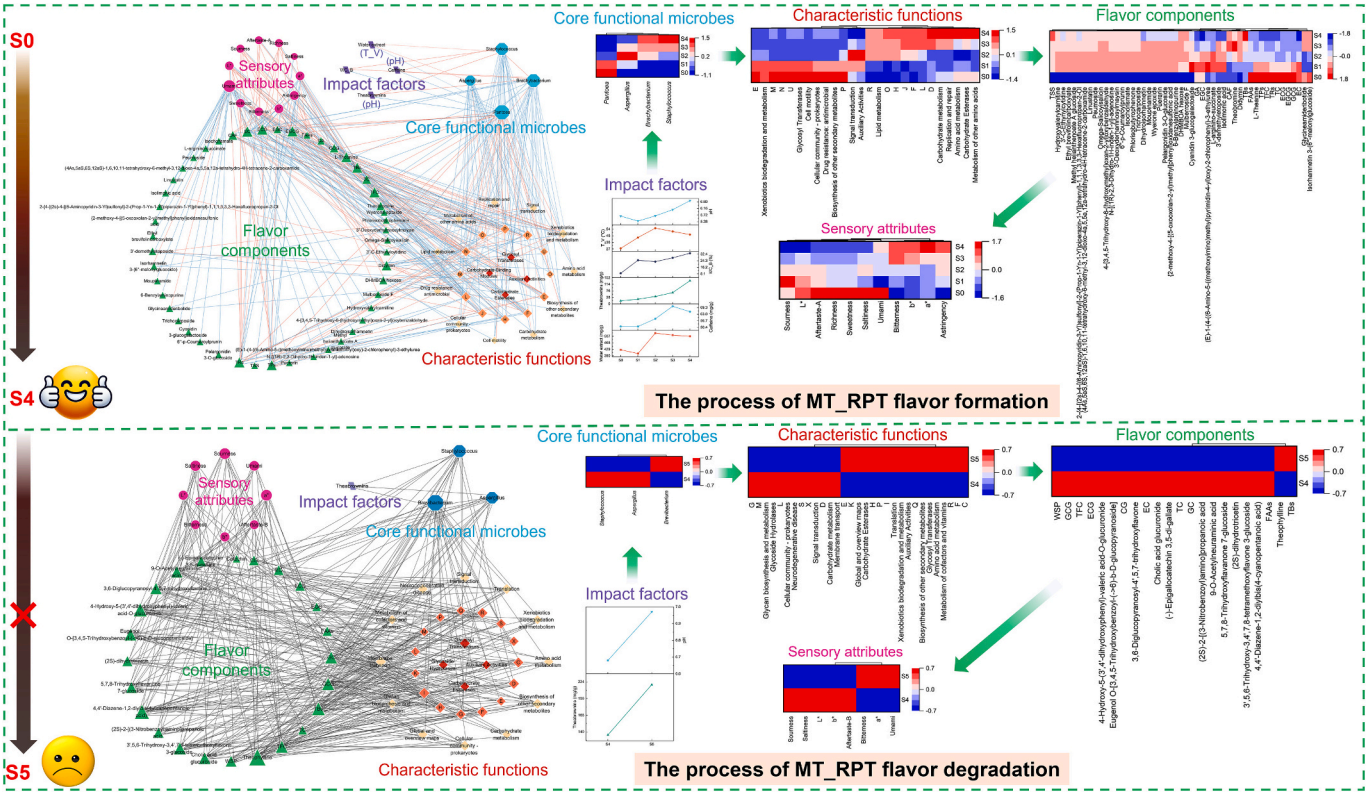

Fig. 8. Associations and dynamics of sensory attributes, key flavor components, characteristic functions, core functional microbes, and impact factors during mellow and thick-type ripened Pu-erh tea formation and degradation.

infusion exhibits a bright orange-red color and a mellow taste, though slight sourness and astringency persist.

In the late fermentation stage (19–24 days), microbial functions primarily involve nucleotide metabolism, DNA replication and repair, coenzyme transport, and the accumulation of key metabolites, including carbohydrates, lipids, and amino acids. *Aspergillus* levels decline significantly, while *Brachybacterium* and *Staphylococcus* proliferate, becoming the dominant microbes. These core functional microbes collectively contribute to substantial decreases in FAAs, CAF, theobromine, TPs, TFC, TC, GA, catechins (EC, ECG, EGC, EGCG), and TRs, while TSS and TBs increase. These shifts in key flavor compounds further enhance a* and b*, as well as umami and astringency, while L*, sourness, sweetness, bitterness, saltiness, aftertaste-A, and richness decrease. By the 24th day (S4), the tea infusion develops a bright auburn-red color and a mellow, thick taste, achieving the highest sensory score.

In the final fermentation stage (25–30 days), microbial functions primarily involve energy management, amino acid metabolism, transcriptional regulation, and various enzymatic activities. *Staphylococcus* and *Aspergillus* decrease, while *Brevibacterium* significantly increases, becoming the dominant microbe. *Brevibacterium* contributes to substantial reductions in WSP, FAAs, TFC, TC, catechins (CG, EC, ECG, GC, GCG), and 11 metabolites, including (−)-epigallocatechin 3,5-di-gallate and 3′,5,6-trihydroxy-3,4′,7,8-tetramethoxyflavone 3-glucoside, while TBs and theophylline increase excessively. These changes in key compounds increase in a*, bitterness, and umami, while L*, b*, sourness, saltiness, and aftertaste-B decrease. By the 30th day (S5), the tea infusion takes on a slightly darker reddish auburn hue, with a taste that lacks mellowness and thickness, accompanied by mild bitterness, leading to a significant decline in sensory score.

In summary, the future fermentation parameter control strategy for MT_RPT production can be outlined as follows: During the early fermentation stage, increasing the central temperature of the tea pile, raising moisture content, and lowering pH can suppress *Pantoea* while promoting the growth and proliferation of *Aspergillus*. In the middle and mid-late fermentation stages, further increasing the central temperature can accelerate *Aspergillus* proliferation, enhancing WE, CAF, and TBs levels. During the late fermentation stages, appropriately lowering the central temperature helps reduce *Aspergillus* while facilitating the growth of *Brachybacterium* and *Staphylococcus*, further increasing TBs levels. Additionally, in compliance with CNIS GB/T 22111–2008, controlling TBs content within 140 mg/g is essential to ensure optimal MT_RPT quality and complete fermentation.

4. Conclusion

This study investigates the flavor formation of MT_RPT during basket-type fermentation using sensory evaluation, multi-omics analysis, and multivariate statistical methods. The sensory evaluation identified day 24 as the optimal time for flavor development, characterized by a bright auburn-red infusion and a mellow, thick taste. However, over-fermentation on day 30 led to flavor degradation, evidenced by increased bitterness and reduced mellowness. Absolute quantification of chemical components and non-targeted metabolomics analysis revealed a significant increase in five key chemical compounds (TBs, TSS, EC, CAF, and theobromine), while 11 other compounds decreased, and 33 nonvolatile metabolites exhibited significant differences. These compounds were closely linked to the formation of the mellow flavor. At the final fermentation stage, reductions in WSP, FAAs, and 11 metabolites, along with increased TBs and theophylline, were associated with flavor degradation. Metagenomic analysis revealed that *Pantoea* and *Aspergillus* dominated the early and mid-fermentation stages, respectively, while *Brachybacterium* and *Staphylococcus* were prevalent in the late fermentation stages. These microbiomarkers facilitated the formation of a mellow and thick flavor, while an increase in *Brevibacterium* was closely associated with flavor degradation. Additionally, this study highlights the critical role of fermentation

parameters, including temperature, moisture content, and pH, in shaping the microbial community and flavor profile. These findings provide valuable insights into optimizing the off-ground fermentation process and standardizing MT_RPT production.

Ethical statement and sensory consent

Before the sensory evaluation, panelists provided informed consent by affirming: "I have carefully read the provided information and fully understand my rights as a participant in this research study. I acknowledge that my responses will be kept confidential, and I voluntarily consent to participate in this study."

CRediT authorship contribution statement

Zixi Yang: Writing – original draft, Software, Methodology, Investigation, Data curation, Conceptualization. **Yanxia Xie:** Methodology, Investigation, Data curation. **Yuanmin Zhu:** Supervision, Resources, Conceptualization. **Mengjie Lei:** Software, Data curation. **Xuemin Chen:** Visualization, Methodology. **Wenwen Jin:** Software, Resources. **Chunhua Fu:** Software, Resources. **Longjiang Yu:** Writing – review & editing, Supervision, Resources, Project administration, Investigation, Conceptualization.

Declaration of competing interest

The authors declare that they have no known competing financial interests or personal relationships that could have appeared to influence the work reported in this paper.

Acknowledgments

This work was supported by the National Key Research and Development Program of China (2023YFD2100902), the Fundamental Research Funds for the Central Universities (2023XCZX001), and the Yunnan Academician (Expert) Workstation (202205AF150090).

Appendix A. Supplementary data

Supplementary data to this article can be found online at https://doi.org/10.1016/j.fochx.2025.102424.

Data availability

Data will be made available on request.

References

Bian, X., Miao, W., Zhao, M., Zhao, Y., Xiao, Y., Li, N., & Wu, J. (2022). Microbiota drive insoluble polysaccharides utilization via microbiome-metabolome interplay during Pu-erh tea fermentation. *Food Chemistry, 377*, Article 132007. https://doi.org/10.1016/j.foodchem.2021.132007

Bradford, M. M. (1976). A rapid and sensitive method for the quantitation of microgram quantities of protein utilizing the principle of protein-dye binding. *Analytical Biochemistry, 72*(1), 248–254. https://doi.org/10.1016/0003-2697(76)90527-3

Buchfink, B., Xie, C., & Huson, D. H. (2015). Fast and sensitive protein alignment using DIAMOND. *Nature Methods, 12*(1), 59–60. https://doi.org/10.1038/nmeth.3176

Cao, L., Guo, X., Liu, G., Song, Y., Ho, C., Hou, R., … Wan, X. (2018). A comparative analysis for the volatile compounds of various Chinese dark teas using combinatory metabolomics and fungal solid-state fermentation. *Journal of Food and Drug Analysis, 26*(1), 112–123. https://doi.org/10.1016/j.jfda.2016.11.020

Cao, Q., Zou, C., Zhang, Y., Du, Q., Yin, J., Shi, J., … Xu, Y. (2019). Improving the taste of autumn green tea with tannase. *Food Chemistry, 277*, 432–437. https://doi.org/10.1016/j.foodchem.2018.10.146

Chen, S., Yang, Z., Sun, W., Tian, K., Sun, P., & Wu, J. (2024). TMV-CP based rational design and discovery of α-amide phosphate derivatives as anti plant viral agents. *Bioorganic Chemistry, 147*, Article 107415. https://doi.org/10.1016/j.bioorg.2024.107415

Cheng, L., Peng, L., Li, X., Xu, L., Chen, J., Zhu, Y., … Wei, X. (2024). Co-occurrence network and functional profiling of the bacterial community in the industrial pile fermentation of Qingzhuan tea: Understanding core functional bacteria. *Food Chemistry, 454*, Article 139658. https://doi.org/10.1016/j.foodchem.2024.139658

Cheng, L., Wang, Y., Zhang, J., Xu, L., Zhou, H., Wei, K., … Wei, X. (2021). Integration of non-targeted metabolomics and E-tongue evaluation reveals the chemical variation and taste characteristics of five typical dark teas. *LWT, 150*, Article 111875. https://doi.org/10.1016/j.lwt.2021.111875

Deng, S., Zhang, T., Fan, S., Na, H., Dong, H., Wang, B., … Liu, X. (2024). Polysaccharide conjugates' contribution to mellow and thick taste of Pu-erh ripe tea, besides Theabrownin. *Food Chemistry: X, 23*, Article 101726. https://doi.org/10.1016/j.fochx.2024.101726

Deng, S., Zhou, X., Dong, H., Xu, Y., Gao, Y., Wang, B., & Liu, X. (2022). Mellow and thick taste of Pu−Erh ripe tea based on chemical properties by sensory−Directed flavor analysis. *Foods, 11*(15), 2285. https://www.mdpi.com/2304-8158/11/15/2285.

Du, Y., Tian, Q., Li, G., Yi, J., Hu, X., & Jiang, Y. (2024). Advanced application of slightly acidic electrolyzed water for fresh-cut fruits and vegetables preservation. *Food Research International, 195*, Article 114996. https://doi.org/10.1016/j.foodres.2024.114996

DuBois, M., Gilles, K. A., Hamilton, J. K., Rebers, P. A., & Smith, F. (1956). Colorimetric method for determination of sugars and related substances. *Analytical Chemistry, 28*(3), 350–356. https://doi.org/10.1021/ac60111a017

Ge, Y., Li, N., Fu, Y., Yu, X., Xiao, Y., Tang, Z., … Jiang, Z. (2021). Deciphering superior quality of Pu-erh tea from thousands of years' old trees based on the chemical profile. *Food Chemistry, 358*, Article 129602. https://doi.org/10.1016/j.foodchem.2021.129602

He, S., Deng, X., Han, Y., Gong, Z., Wang, J., Tao, X., … Chen, Y. (2023). Metabolites and metagenomic analysis reveals the quality of Pu-erh "tea head". *Food Chemistry, 429*, Article 136992. https://doi.org/10.1016/j.foodchem.2023.136992

Hu, J., Feng, X., Song, H., Hao, Z., Ma, S., Hu, H., … Chu, Q. (2024). Enzymatic reactions throughout cultivation, processing, storage and post-processing: Progressive sculpture of tea quality. *Trends in Food Science & Technology, 143*, Article 104294. https://doi.org/10.1016/j.tifs.2023.104294

Hu, S., Li, X., Gao, C., Meng, X., Li, M., Li, Y., … Hao, Q. (2022). Detection of composition of functional component theabrownins in Pu-erh tea by degradation method. *Food Science and Human Wellness, 11*(3), 643–647. https://doi.org/10.1016/j.fshw.2021.12.021

Huang, F., Zheng, X., Ma, X., Jiang, R., Zhou, W., Zhou, S., … Jia, W. (2019). Theabrownin from Pu-erh tea attenuates hypercholesterolemia via modulation of gut microbiota and bile acid metabolism. *Nature Communications, 10*(1), 4971. https://doi.org/10.1038/s41467-019-12896-x

Huang, H., Wu, N., Liang, Y., Peng, X., & Shu, J. (2022). SLNL: A novel method for gene selection and phenotype classification. *International Journal of Intelligent Systems, 37*(9), 6283–6304. https://doi.org/10.1002/int.22844

Li, H., He, R., Xiong, X., Zhang, M., Yang, T., Jiang, Z., … Ma, X. (2016). Dynamic diversification of bacterial functional groups in the Baiyunbian liquor stacking fermentation process. *Annals of Microbiology, 66*(3), 1229–1237. https://doi.org/10.1007/s13213-016-1211-9

Li, H., Luo, L., Wang, J., Fu, D., & Zeng, L. (2019). Lexicon development and quantitative descriptive analysis of Hunan Fuzhuan brick tea infusion. *Food Research International, 120*, 275–284. https://doi.org/10.1016/j.foodres.2019.02.047

Li, Q., Huang, J., Li, Y., Zhang, Y., Luo, Y., Chen, Y., … Liu, Z. (2017). Fungal community succession and major components change during manufacturing process of Fu brick tea. *Scientific Reports, 7*(1), 6947. https://doi.org/10.1038/s41598-017-07098-8

Li, T., Lu, C., Huang, J., Chen, Y., Zhang, J., Wei, Y., … Ning, J. (2022). Qualitative and quantitative analysis of the pile fermentation degree of Pu-erh tea. *LWT, 173*, Article 114327. https://doi.org/10.1016/j.lwt.2022.114327

Li, T., Wei, Y., Feng, W., Lu, M., Ke, H., Li, Y., … Ning, J. (2023). Exploring the mysterious effect of piling fermentation on Pu-erh tea quality formation: Microbial action and moist-heat action. *LWT, 185*, Article 115132. https://doi.org/10.1016/j.lwt.2023.115132

Li, T., Zhang, Y., Jia, H., Zhang, J., Wei, Y., Deng, W., & Ning, J. (2022). Effects of microbial action and moist-heat action on the nonvolatile components of Pu-erh tea, as revealed by metabolomics. *Journal of Agricultural and Food Chemistry, 70*(49), 15602–15613. https://doi.org/10.1021/acs.jafc.2c05925

Li, Y. (2021). Study on fermentation technology of three-dimensional numerical control small basket of mature ripened Pu-erh tea. *New Agriculture, 6*, 27–28.

Li, Y., Li, Y., Xiao, T., Jia, H., Xiao, Y., Liu, Z., … Zhu, M. (2024). Integration of non-targeted/targeted metabolomics and electronic sensor technology reveals the chemical and sensor variation in 12 representative yellow teas. *Food Chemistry: X, 21*, Article 101093. https://doi.org/10.1016/j.fochx.2023.101093

Li, Y., Zhu, G., Zhou, H., Huang, Y., Zhao, Y., & Hao, Q. (2013). Optimization of technology for fermenting Pu-erh tea with automatic fermentation tank. *Food and Fermentation Industries, 39*(09), 89–94. https://doi.org/10.13995/j.cnki.11-1802/ts.2013.09.028

Li, Z., Feng, C., Luo, X., Yao, H., Zhang, D., & Zhang, T. (2018). Revealing the influence of microbiota on the quality of Pu-erh tea during the fermentation process by shotgun metagenomic and metabolomic analysis. *Food Microbiology, 76*, 405–415. https://doi.org/10.1016/j.fm.2018.07.001

Liang, H., Zhu, Z., Fan, Y., Hu, J., Wu, J., Mu, Z., … Li, S. (2024). Integrated microbiomic and metabolomic dynamics of Yi traditional fermented liquor. *Food Chemistry: X, 24*, Article 102016. https://doi.org/10.1016/j.fochx.2024.102016

Lin, Y., Huang, Y., Liu, X., Pan, Y., Feng, X., Guo, H., … Chu, Q. (2024). Uncovering the Shuixian tea grades hierarchy in Chinese national standard: From sensory evaluation to microstructure and volatile compounds analysis. *Food Chemistry, 459*, Article 140342. https://doi.org/10.1016/j.foodchem.2024.140342

Liu, Y., Luo, L., Liao, C., Chen, L., Wang, J., & Zeng, L. (2018). Effects of brewing conditions on the phytochemical composition, sensory qualities and antioxidant activity of green tea infusion: A study using response surface methodology. *Food Chemistry, 269*, 24–34. https://doi.org/10.1016/j.foodchem.2018.06.130

Liu, Z., Guo, Z., Zhou, J., Guo, X., & Chen, Y. (2024). Biotic interactions and environmental modifications determine symbiotic microbial diversity and stability. *Computational and Structural Biotechnology Journal, 23*, 2717–2726. https://doi.org/10.1016/j.csbj.2024.05.047

Long, J., Chen, C., Wang, Y., Deng, H., Zhang, Q., Huang, L., … Zhu, P. (2024). Exploring the microbial community, physicochemical properties, metabolic characteristics, and pathways during tank fermentation of Liupao tea. *LWT, 204*, Article 116449. https://doi.org/10.1016/j.lwt.2024.116449

Long, P., Li, Y., Han, Z., Zhu, M., Zhai, X., Jiang, Z., … Zhang, L. (2024). Discovery of color compounds: Integrated multispectral omics on exploring critical colorant compounds of black tea infusion. *Food Chemistry, 432*, Article 137185. https://doi.org/10.1016/j.foodchem.2023.137185

Long, P., Wen, M., Granato, D., Zhou, J., Wu, Y., Hou, Y., & Zhang, L. (2020). Untargeted and targeted metabolomics reveal the chemical characteristics of pu-erh tea (*Camellia assamica*) during pile-fermentation. *Food Chemistry, 311*, Article 125895. https://doi.org/10.1016/j.foodchem.2019.125895

Ma, C., Ma, B., Zhou, B., Xu, L., Hu, Z., Li, X., & Chen, X. (2024). Pile-fermentation mechanism of ripened Pu-erh tea: Omics approach, chemical variation and microbial effect. *Trends in Food Science & Technology, 146*, Article 104379. https://doi.org/10.1016/j.tifs.2024.104379

Ma, C., Zhou, B., Wang, J., Ma, B., Lv, X., Chen, X., & Li, X. (2023). Investigation and dynamic changes of phenolic compounds during a new-type fermentation for ripened Pu-erh tea processing. *LWT, 180*, Article 114683. https://doi.org/10.1016/j.lwt.2023.114683

Ma, Y., Wei, Z., Xiao, X., Yu, K., Huang, H., Tan, J., … Li, Y. (2024). Investigating the impact of various sorghum types on the key aroma compounds of Sichuan Xiaoqu baijiu through application of the sensomics approach. *Food Chemistry: X, 22*, Article 101367. https://doi.org/10.1016/j.fochx.2024.101367

Mohammadi, N., Esteki, M., & Simal-Gandara, J. (2024). Machine learning for authentication of black tea from narrow-geographic origins: Combination of PCA and PLS with LDA and SVM classifiers. *LWT, 203*, Article 116401. https://doi.org/10.1016/j.lwt.2024.116401

Pang, B., Huang, L., Teng, J., Zhang, J., Xia, N., & Wei, B. (2021). Effect of pile fermentation on the cells of Chinese Liupao tea: The first record of cell wall of Liupao tea on transmission electron microscope. *Food Chemistry, 361*, Article 130034. https://doi.org/10.1016/j.foodchem.2021.130034

Van Soest, P. J. (1978). Dietary fibers: Their definition and nutritional properties12. *The American Journal of Clinical Nutrition, 31*(10, Supplement 1), S12–S20. https://doi.org/10.1093/ajcn/31.10.S12

Wang, M., Zhang, S., Li, R., & Zhao, Q. (2024). Unraveling the specialized metabolic pathways in medicinal plant genomes: A review. *Frontiers in Plant Science, 15*, 1459533. https://doi.org/10.3389/fpls.2024.1459533

Wang, S., Qiu, Y., Gan, R., & Zhu, F. (2022). Chemical constituents and biological properties of Pu-erh tea. *Food Research International, 154*, Article 110899. https://doi.org/10.1016/j.foodres.2021.110899

Wang, T., Li, R., Liu, K., Chen, Q., Bo, N., Wang, Q., … Zhao, M. (2023). Changes in sensory characteristics, chemical composition and microbial succession during fermentation of ancient plants Pu-erh tea. *Food Chemistry: X, 20*, Article 101003. https://doi.org/10.1016/j.fochx.2023.101003

Wang, T., Li, X., Yang, H., Wang, F., Kong, J., Qiu, D., & Li, Z. (2018). Mass spectrometry-based metabolomics and chemometric analysis of Pu-erh teas of various origins. *Food Chemistry, 268*, 271–278. https://doi.org/10.1016/j.foodchem.2018.06.041

Wang, X., Li, X., Liu, B., Long, F., Wei, J., Zhang, Y., … Yue, T. (2021). Comparison of chemical constituents of *Eurotium cristatum*-mediated pure and mixed fermentation in summer-autumn tea. *LWT, 143*, Article 111132. https://doi.org/10.1016/j.lwt.2021.111132

Wang, X., Nian, B., Duan, S., Yan, L., Yang, R., Cui, T., … Luo, C. (2017). Comparison on chemical compounds and antioxidant activity of pu-erh tea fermented by numerical control and traditional methods. *Food and Fermentation Industries, 43*(05), 138–143. https://doi.org/10.13995/j.cnki.11-1802/ts.201705022

Wang, Y., Guo, S., Sun, W., Tu, H., Tang, Y., Xu, Y., … Wu, J. (2024). Synthesis of 4H-pyrazolo[3,4-d]pyrimidin-4-one hydrazine derivatives as a potential inhibitor for the self-assembly of TMV particles. *Journal of Agricultural and Food Chemistry, 72*(6), 2879–2887. https://doi.org/10.1021/acs.jafc.3c05334

Wang, Z., Li, H., Huang, W., Duan, S., Yan, Y., Zeng, Z., … Liu, Y. (2024). Landscapes of the main components, metabolic and microbial signatures, and their correlations during pile-fermentation of Tibetan tea. *Food Chemistry, 430*, Article 136932. https://doi.org/10.1016/j.foodchem.2023.136932

Wang, Z., Liang, Y., Gao, C., Wu, W., Kong, J., Zhou, Z., … Sun, W. (2024). The flavor characteristics and antioxidant capability of aged Jinhua white tea and the mechanisms of its dynamic evolution during long-term aging. *Food Chemistry, 436*, Article 137705. https://doi.org/10.1016/j.foodchem.2023.137705

Wang, Z., Zhang, Y., Tong, X., & Liu, Z. (1991). Changes of tea polyphenols and carbohydrates in the initial production of dark tea. *Journal of Tea Science*, (S1), 23–28.

Xiao, L., Yang, C., Zhang, X., Wang, Y., Li, Z., Chen, Y., … Xiao, Y. (2023). Effects of solid-state fermentation with *Bacillus subtilis* LK-1 on the volatile profile, catechins composition and antioxidant activity of dark teas. *Food Chemistry: X, 19*, Article 100811. https://doi.org/10.1016/j.fochx.2023.100811

Xiong, S., Xu, X., Zhang, L., Du, T., Huang, T., Huang, J., … Xie, M. (2024). Integrated metatranscriptomics and metabolomics reveal microbial succession and flavor formation mechanisms during the spontaneous fermentation of Laotan Suancai. *Food Research International, 177*, Article 113865. https://doi.org/10.1016/j.foodres.2023.113865

Yang, X., Xia, X., Zhang, Z., Nong, B., Zeng, Y., Wu, Y., … Li, D. (2019). Identification of anthocyanin biosynthesis genes in rice pericarp using PCAMP. *Plant Biotechnology Journal, 17*(9), 1700–1702. https://doi.org/10.1111/pbi.13133

Ye, J., Ye, Y., Yin, J., Jin, J., Liang, Y., Liu, R., … Xu, Y. (2022). Bitterness and astringency of tea leaves and products: Formation mechanism and reducing strategies. *Trends in Food Science & Technology, 123*, 130–143. https://doi.org/10.1016/j.tifs.2022.02.031

Zhang, L., Zhang, Z., Zhou, Y., Ling, T., & Wan, X. (2013). Chinese dark teas: Post-fermentation, chemistry and biological activities. *Food Research International, 53*(2), 600–607. https://doi.org/10.1016/j.foodres.2013.01.016

Zhang, M., Guo, D., Wang, H., Wu, G., Shi, Y., Zheng, T., … Li, X. (2024). Evaluation of microbial and organic metabolite characteristics in fermented tobacco from different grades by comprehensive microbiomes and chemometrics analysis. *Industrial Crops and Products, 222*, Article 119706. https://doi.org/10.1016/j.indcrop.2024.119706

Zhang, S., Liu, S., Li, H., Luo, L., & Zeng, L. (2023). Identification of the key phytochemical components responsible for sensory characteristics of Hunan Fuzhuan brick tea. *Journal of Food Composition and Analysis, 120*, Article 105289. https://doi.org/10.1016/j.jfca.2023.105289

Zhang, Z., Fan, H., Yu, Z., Luo, X., Zhao, J., Wang, N., & Li, Z. (2024). Metagenomics-based gene exploration and biochemical characterization of novel glucoamylases and α-amylases in Daqu and Pu-erh tea microorganisms. *International Journal of Biological Macromolecules, 278*, Article 134182. https://doi.org/10.1016/j.ijbiomac.2024.134182

Zhu, L., Liao, R., Wu, N., Zhu, G., & Yang, C. (2019). Heat stress mediates changes in fecal microbiome and functional pathways of laying hens. *Applied Microbiology and Biotechnology, 103*(1), 461–472. https://doi.org/10.1007/s00253-018-9465-8

Zhu, M., Li, N., Zhou, F., Ouyang, J., Lu, D., Xu, W., … Wu, J. (2020). Microbial bioconversion of the chemical components in dark tea. *Food Chemistry, 312*, Article 126043. https://doi.org/10.1016/j.foodchem.2019.126043